

Altered intratumoral immune composition after Nivolumab treatment in patients with recurrent glioblastoma

Sine Hadrup (✉ sirha@dtu.dk)

Section for Experimental and Translational Immunology, Department of Health Technology, Technical University of Denmark, Lyngby

Signe Skadborg

Section for Experimental and Translational Immunology, Department of Health Technology, Technical University of Denmark, Lyngby

Simone Maarup

Rigshospitalet

Arianna Draghi

National Center for Cancer Immune Therapy, Department of Oncology, Copenhagen University Hospital Herlev <https://orcid.org/0000-0002-5894-6750>

Annie Borch

Section for Experimental and Translational Immunology, Department of Health Technology, Technical University of Denmark, Lyngby

Sille Hendriksen

Section for Experimental and Translational Immunology, Department of Health Technology, Technical University of Denmark, Lyngby

Filip Mundt

Broad Institute <https://orcid.org/0000-0001-8622-2971>

Matthias Mann

University of Copenhagen

Jane Skjoeth-Rasmussen

Christina Westmose Yde

Copenhagen University Hospital

Hans Poulsen

Rigshospitalet

Benedikte Hasselbach

Rigshospitalet

Inge Marie Svane

Center for Cancer Immune Therapy and Department of Oncology, Herlev Hospital, University of Copenhagen <https://orcid.org/0000-0002-9451-6037>

Ulrik Lassen


Rigshospitalet, Copenhagen, Denmark <https://orcid.org/0000-0002-3865-4574>

Article

Keywords: Cancer immunotherapy, Glioblastoma Multiforme, T-cells, Immune Checkpoint Blockade, Neoantigens

Posted Date: July 6th, 2023

DOI: <https://doi.org/10.21203/rs.3.rs-2976894/v1>

License:  This work is licensed under a Creative Commons Attribution 4.0 International License.
[Read Full License](#)

Additional Declarations: **Yes** there is potential Competing Interest. Nivolumab was provided by Bristol-Meyer Squibb. Bristol-Meyer Squibb did not exert any influence on the study and did not provide financial support for the study. SRH is the cofounder of PokeAcell and is the coinventor of patents WO2015185067 (Determining antigen recognition through barcoding of MHC multimers) and WO2015188839 (General detection and isolation of specific cells by binding of labeled molecules) for the barcoded MHC technology that is licensed to Immudex. IMS has received grants from or signed contracts with Bristol-Myers Squibb, Adaptimmune, IO Biotech, Lytix biopharma, TILT Biotherapeutics, and Enara Bio; has received consulting fees from MSD, IO Biotech, Novartis, Pierre Fabre, Novo Nordisk, and TILT Biotherapeutics; has received honoraria for lectures, presentations, or educational events from MSD, Novartis, Sanofi Aventis, Pierre Fabre, Bristol-Myers Squibb, IO Biotech, TILT Biotherapeutics, Novo Nordisk, and Takeda; has received support for attending meetings and/or travel from MSD; owns IO Biotech stocks.

Altered intratumoral immune composition after Nivolumab treatment in patients with recurrent glioblastoma

Signe Koggersbøl Skadborg^{1,9} Simone Maarup^{2,3,9}, Arianna Draghi³, Annie Borch¹, Sille Hendriksen¹, Filip Mundt⁴, Vilde Pedersen^{2,7,8}, Matthias Mann⁴, Ib Jarle Christensen², Jane Skjøth-Ramussen^{2,5}, Christina Westmose Yde⁶, Bjarne Winther Kristensen^{2,7,8}, Hans Skovgaard Poulsen², Benedikte Hasselbalch², Inge Marie Svane³, Ulrik Lassen^{2,9}, Sine Reker Hadrup^{1,9}

¹ Experimental and Translational Immunology, Department of Health Technology, Technical University of Denmark, Kgs. Lyngby, Denmark

² DCCC Brain Tumor Center, Department of Oncology, Copenhagen University Hospital Rigshospitalet, Copenhagen, Denmark

³ National Center for Cancer Immune Therapy, CCIT-DK, Copenhagen University Hospital Herlev Hospital, Herlev, Denmark

⁴ Novo Nordisk Foundation Center for Protein Research, CPR, Copenhagen University, Copenhagen Denmark

⁵ Neurosurgical Department, Copenhagen University Hospital, Copenhagen, Denmark

⁶ Center for Genomic Medicine, Copenhagen University Hospital, Copenhagen, Denmark

⁷ Department of Pathology, The Bartholin Institute, Rigshospitalet, Copenhagen University Hospital, Copenhagen, Denmark

⁸ Department of Clinical Medicine and Biotech Research & Innovation Centre (BRIC), University of Copenhagen, Copenhagen, Denmark

⁹ These authors contributed equally: Signe Koggersbøl Skadborg, Simone Maarup, Ulrik Lassen, Sine Reker Hadrup

Keywords: Cancer immunotherapy, Glioblastoma Multiforme, T-cells, Immune Checkpoint Blockade, Neoantigens

Abstract

Glioblastoma is an aggressive brain tumor with poor prognosis, and consequently immunotherapy is being explored as a potential treatment option. However, it is unclear whether systemic immunotherapy can reach and modify the tumor microenvironment in the brain. We evaluated immune characteristics in tumor and blood samples from recurrent glioblastoma patients, who received Nivolumab and Bevacizumab. One group received Nivolumab one week prior to surgery, and immune characteristics of the tumor were compared to control patients receiving salvage resection without prior Nivolumab treatment. Nivolumab-bound T-cells could be detected in tumor tissue, along with increasing numbers of both activated and differentiated CD4+ and CD8+ T-cells. An associated upregulation of co-inhibitory receptors on T-cells was observed following Nivolumab treatment. Additionally, tumor-reactivity was detected in tumor infiltrating lymphocytes (TILs) from Nivolumab-treated patients, and neoantigen-reactive T-cells could be identified in both TILs and blood, indicating a systemic response towards GBM in a subset of patients.

1 Introduction

2 At primary diagnosis, glioblastoma (GBM) patients are treated with maximal surgery, radiation and
3 concomitant Temozolomide, also known as Stupp's regimen¹. However, when relapse occur no standard
4 treatment is available ². Even though numerous treatment strategies have been explored, overall survival
5 (OS) remains at 14.6 months ¹. Therefore, new treatment options are urgently needed, and
6 immunotherapy is one strategy being explored, that may show promise in selected patients ^{3,4}.

7 The brain is determined as an immune privileged organ, which has been equated with no passage of
8 peripheral immune cells to the parenchyma of the brain ⁵. However, it has been shown that
9 communication with the peripheral immune system occurs, including cellular exchange. It is known that
10 T-cells can be primed in the meningeal area of the brain ⁶. However, knowledge of the route of entry and
11 presence of effector T-cells in the parenchyma or tumor tissue localized in the brain, is minimal. It has
12 been shown in mice that cerebral spinal fluid (CSF) and interstitial fluid are drained via central nervous
13 system (CNS) draining lymphatic vessel to the deep cervical lymph node, which suggests an alternative
14 route for immune surveillance of the brain ⁷⁻⁹.

15 Immunotherapy has revolutionized cancer treatment, yet many cancer types are still unresponsive to
16 current immunotherapeutic strategies ¹⁰⁻¹². The effect of immune-checkpoint inhibition has been sparse
17 in GBM and it has been questioned, if the checkpoint inhibitors pass the blood brain barrier (BBB)
18 sufficiently to enter the tumor microenvironment ¹³. Nivolumab is a molecule of 146 kDa, while only
19 molecules of 0.4-0.5 kDa are believed to pass the BBB freely ¹³. It has earlier been shown that the BBB is
20 compromised in some areas of primary brain tumors while other areas remain intact ^{14,15}. Additionally,
21 some glioblastoma tumors have high collagen levels, which can challenge the penetration capacity ¹⁶.
22 Together these characteristics may limit the penetrance of Nivolumab and effector immune cells and
23 hence compromise the effect of immunotherapy in GBM.

24 Checkpoint inhibitors have shown promising results in brain cancer in mouse models ^{17,18}, but when the
25 treatment is translated to the human setting, the responses have waned ¹⁹. Therefore, it is of great
26 importance to understand the influence of checkpoint inhibition on a cellular level in GBM. In this study,
27 we explored the intratumoral presence of Nivolumab and its effect on the phenotypic profile of
28 intratumoral and peripheral T-cells as a window of opportunity in patients with relapsed GBM undergoing
29 surgery. Tumors were surgically resected seven days after receiving first-dose of Nivolumab treatment.

- 1 We then examined the tumor reactivity of expanded tumor infiltrated lymphocytes (TILs) and the
- 2 presence of neoantigen-reactive CD8+ T-cells in GBM lesions and peripheral blood.

Results

Clinical setup and sample collection

In the presented study, an open-label phase 2 clinical study – CA209-9UP, 44 patients with recurrent GBM following Stupp's regime¹ were included from November 2018 to January 2022; 4 patients became screen failures, while 40 patients were treated with Nivolumab (PD-1 inhibitor) and Bevacizumab (anti-VEGF-A) every 14 days. The patients were divided in two groups; 20 patients received first-dose of 240 mg Nivolumab seven days before salvage resection as a window of opportunity to study treatment effects in tumor tissue (surgical group), while 20 patients were considered non-operable (non-surgical group) (Figure 1a, Supplementary Figure 1).

Clinical data from a historical patient group with recurrent GBM (treated at Rigshospitalet, Denmark, 2006–2014) were used for comparison to investigate potential statistically significant survival benefits of the Nivolumab/Bevacizumab treatment. Additionally, fresh tumor samples were collected following neurosurgery from 10 other control patients with recurrent glioblastoma, not treated with Nivolumab or Bevacizumab, to investigate if Nivolumab could influence the immune-cellular signatures at the tumor site in recurrent GBM patients (Figure 1a).

Tumor and blood samples were collected from all Nivolumab/Bevacizumab-treated patients. From the surgical group (also referred to as NIVO), we collected tumor samples resulting in 19 tumor digests, 15 young TIL cultures (YTILs), 16 rapidly-expanded TIL cultures (REP TILs). Additionally, tumor samples from control patients resulted in 10 tumor digests, 8 YTILs, and 10 REP TILs (Supplementary Table 1).

Intratumoral T-cells from NIVO patients were compared to intratumoral T-cells from control patients. Blood samples were additionally studied for the long-term effect of combination therapy with Nivolumab and Bevacizumab and to examine the role of continuous tumor presence (non-surgical group) versus tumor removal (surgical group).

Patient characteristics, safety and survival benefits

Median age at diagnosis was 57.5 years (surgical group) and 50.5 years (non-surgical group). For both groups, 77% (31 out of 40 patients) did not receive corticosteroids at inclusion (Supplementary Table 2). Tumor samples were historically verified as GBM, however today eight patients would classify as astrocytoma, IDH-mutant, WHO grade IV according to WHO's recent classification of brain tumors^{2,20}. The groups had equal distributions of gender, performance status and corticosteroid usage, while 45% of

1 patients in the surgical group harbored un-methylated MGMT compared to 55% in the non-surgical group
2 (Supplementary Table 2). Overall, the treatment was well tolerated. One suspected unexpected serious
3 adverse reaction (SUSAR) of posterior reversible encephalopathy syndrome (PRES) was reported and the
4 patient was excluded from further treatment. Serious adverse events of grade 3 and 4 (CTCAE version
5 4.03) are listed in Supplementary Table 3.

6 For all 40 patients included in the CA209-9UP clinical trial, we found a median overall survival (mOS) of
7 10.9 months (7.0-14.1) and median progression free survival (mPFS) of 4.1 months (3.8-5.9). When
8 stratified, the surgical and non-surgical group had a mPFS of 6.0 and 3.8 months, respectively, while the
9 mOS was 14.0 months and 6.4 months, respectively. mOS follow-up was 30.0 months (15.2–40.1) and
10 27.2 months (16.0–41.0) in the surgical and non-surgical group, respectively. Multivariate analysis was
11 performed by the following variables: corticosteroid use, MGMT status, gender, age at diagnosis, and
12 treatment group (Supplementary Table 4). Corticosteroid use at inclusion was a significant negative
13 predictor of outcome ($p=0.04$). In a follow-up survival analysis, we removed these patients, but no
14 difference was observed, compared to the results from the whole group. We then stratified on differences
15 in corticosteroid use at baseline ($N=40$) and saw that corticosteroid-using patients had mOS of 7.3 months
16 compared to non-corticosteroid-using patients with mOS of 12.2 months.

17 The real-world data on the historical patient group was extracted from our one-site GBM database, from
18 which we have reported before ²¹. Real-world data as controls is an established method which have been
19 reported by many ²². The historical patient group comprised patients treated with Bevacizumab and
20 Irinotecan and possibly neurosurgical resection ($N=156$; 81 patients had a neurosurgical resection, 75
21 patients did not). The historical surgical group ($N=81$) had a mOS of 9.8 months, compared to the mOS of
22 14.0 months in our Nivolumab/Bevacizumab-treated surgical patient group. While a difference was
23 initially observed between the two groups (log-rank of $p=0.08$) (Figure 1b) when the patients cohorts were
24 matched based on propensity scores, including relevant clinical and performance characteristic, no
25 difference was observed (log-rank p -value= 0.46) (Figure 1c). In the non-surgical group, matched historical
26 patient ($N=75$) had a mOS of 7.0 months, while 6.4 month in the Nivolumab/Bevacizumab-treated patient
27 group, hence no difference was observed both neither without, nor with matching based on propensity
28 score (log-rank of $p=0.77$ and $p=0.11$, respectively) (Figure 1d and e). Thus, we found no survival benefit
29 in patients treated with Nivolumab and Bevacizumab compared to matched historical patients. Although
30 no statistical difference was observed based on the propensity matching, we interestingly observed five
31 long-term survival (>20 months after tumor recurrence) patients in the Nivolumab/Bevacizumab-treated

group. This was unexpected based on clinical parameters, such as time from primary diagnosis to progression (4.8 months, 6.7 months, 4.9 months, 14.8 months and 8.7 months) and MGMT- or IDH-status (two MGMT unmethylated, one IDH mutated).

Intratumoral detection of Nivolumab and tissue-resident T-cells

Tumor samples were analyzed to evaluate the ability of Nivolumab to penetrate the tumor microenvironment (TME). To detect Nivolumab binding to PD-1 on T-cell surfaces, we applied a fluorochrome-conjugated anti-IgG4 (algG4), the isotype of Nivolumab, while free PD-1 molecules were determined by a regular fluorochrome-conjugated anti-PD-1 antibody (aPD-1) (Figure 2a). Tumor digests were rested overnight to re-express certain T-cell surface markers lost during tissue digestion. Before rest, T-cells were only binding algG4, indicating all PD-1 molecules were bound to Nivolumab. After rest, T-cells bound both aPD-1 and algG4, indicating surface presence of new PD-1 molecules during the resting period, or loss of Nivolumab binding. Intratumoral T-cells from control patients only bound aPD-1, confirming that IgG4 binding is specific to Nivolumab (Figure 2b and 2c). Tumor digests were stained for CD69 and CD103, markers when co-expressed identify tissue residency, to confirm that T-cells in the tumor digest included tissue-resident T-cells. Both markers were expressed on both CD4+ and CD8+ T-cells in the tumor digest, with no difference in frequencies between NIVO and control patients (Figure 2d). Importantly, CD103 and CD69 co-expression was also detected within Nivolumab-bound T-cells. Additionally, paired histological formalin fixed paraffin embedded (FFPE) sections from primary and recurrent NIVO tumors were stained for PD-1, PD-L1, IgG4 and CD3. Three patients were identified with distinct PD-1+ and IgG4+ cells in the recurrent tumors after Nivolumab treatment, while FFPE sections from the corresponding untreated primary tumors were IgG4 negative (Supplementary Figure 2).

Altogether, this suggests that Nivolumab has penetrated the tumor tissue as free immunoglobulins and can hereby bind to tissue-resident T-cells within the TME (Figure 2e and 2f).

Nivolumab mediates CNS homing and T-cell activation in GBM

Next, we searched for T-cells in both tumor and blood that expressed a CNS homing profile. The chemokine receptors CD183 (CXCR3) and CD195 (CCR5) have previously been correlated with CNS homing in neurological inflammation^{23,24}. As cancer is also an inflammatory disease, we investigated the expression of the two chemokine receptors, CD183 and CD195. The frequency of CD4+ T-cells co-expressing CD183 and CD195 was higher in Nivolumab-treated tumors compared to controls, while stable for CD8+ T-cells (Figure 3a). Furthermore, a significantly increased surface expression of both CD183 and

CD195 was found on CD4+ and CD8+ T-cells in tumors of NIVO patients compared to the control patients, suggesting a treatment related effect (Figure 3b). This coincided with peripheral blood mononuclear cells (PBMCs) showing a trend towards lower frequency of both CD4+ and CD8+ T-cells that co-expresses the two chemokine receptors (Supplementary Figure 3). Together, this suggests that Nivolumab can reinforce CNS T-cell recruitment. Interestingly, in blood we also observed a difference in chemokine expressing CD8+ T-cells between Nivolumab-treated patients who had their tumor removed (surgical group) and the tumor bearing patients (non-surgical group). We found that PBMCs from the non-surgical group had significantly higher frequencies of CD183+ CD195+ T-cells within the CD8+ population at baseline (day 0) and week 16 compared to the surgical group (Figure 3c-d). The larger fraction of this migratory phenotype suggests a more pronounced neurological inflammation in patients in the non-surgical arm.

As we found that a CNS homing potential could be observed among T-cells in both blood and tumor, we further evaluated the activation status of intratumoral T-cells after Nivolumab treatment. T-cells co-expressing CD39, a marker of recent T-cell activation, and CD103 and CD69 were only present in tumor tissue (Figure 3e, Supplementary Figure 3). We found significantly higher frequencies of such activated tissue-resident T-cells within the CD8+ T-cell population in NIVO tumors compared to tumors from control patients. A similar tendency was also found within CD4+ T-cells but in a much lower frequency level (Figure 3e). Tissue-resident T-cells expressing the early activation marker CD137 (4-1BB), were also found in low frequencies within both CD8+ and CD4+ T-cells and tended to increase in CD8+ T-cells after Nivolumab treatment (Figure 3f). Furthermore, the frequency of T-cells in the tumor expressing the co-stimulatory molecule, CD28, did not significantly change with Nivolumab treatment (Figure 3g). However, a large heterogeneity in frequency of such cells was observed among CD8+ T-cells in the Nivolumab-treated group. Interestingly, patients with higher frequency of CD8+ T-cells expressing CD28 tended to have longer progression-free survival (PFS) and overall survival (OS) after recurrence, but only among NIVO patients (Supplementary Figure 4). Additionally, we demonstrated a strong treatment-associated upregulation of the surface expression of CD28 on intratumoral T-cells (Figure 3h). Finally, enhanced proliferation was observed among both intratumoral CD8+ and CD4+ T-cells following Nivolumab treatment, based on the detection of Ki67 expression (Figure 3i).

In summary, intratumoral T-cells, collected seven days after Nivolumab infusion, had an increased CNS-homing profile and a higher frequency of T-cells with status of activation and proliferation compared to intratumoral T-cells from untreated control patients.

Increased intratumoral T-cell differentiation after Nivolumab treatment

T-cell expression of inhibitory molecules and markers of differentiation including PD-1, TIGIT, LAG-3, TIM-3 and CTLA-4 were examined to evaluate potential Nivolumab induced changes in blood (PBMCs) and tumor (digest). PD-1 expression was measured using both aPD-1 and algG4 staining antibodies. The kinetics of Nivolumab binding is shown in Figure 4a, where PBMC derived CD8+ T-cells are stained with aPD-1 and algG4. At baseline, PD-1 molecules on T-cells were stained only by aPD-1, while after Nivolumab administration, PD-1 molecules were instead stained by algG4. The sum of the T-cell populations stained by either aPD-1 or algG4 was therefore defined as the total PD-1+ population, to compare expression of PD-1 between time points and patient groups. A significant drop in frequencies of PD-1 expressing CD8+ T-cells was observed in PBMCs after Nivolumab treatment and a similar trend was observed within CD4+ T-cells (Figure 4b). This drop in PD-1 expressing CD8+ T-cells in the NIVO patients was similarly detected in the tumor (Figure 4c). Overall, Nivolumab appears to induce a downregulation of PD-1 expression in T-cells, or a selective loss of PD-1 expressing T-cells.

When investigating expression of other inhibitory molecules (TIGIT, LAG-3, TIM-3 and CTLA-4), it was observed that the loss of PD-1 expression seems to be counteracted by a general increase in these checkpoint molecules. Higher frequencies of T-cells expressing TIGIT, LAG-3, TIM-3 and CTLA-4 were observed in tumor tissue from NIVO patients compared to untreated control patients. The frequencies of T-cells expressing TIGIT were significantly higher in tumors following Nivolumab treatment, both in the CD8+ and CD4+ T-cells populations (Figure 4d). Interestingly, when comparing the frequency of TIGIT+ T-cells in blood between the surgical group and non-surgical group of Nivolumab-treated patients, significantly higher frequencies of CD8+ T-cells expressing TIGIT were found in the non-surgical group at week 16 (Figure 4e). This could indicate that there was an ongoing exhaustion of T-cells in the non-surgical group, as the tumor was still present and chronic inflammation within the tumor tissue could be monitored by a peripheral upregulation of TIGIT. Moreover, there was a significantly higher percentage of T-cells expressing LAG-3, TIM-3 (CD8+) and CTLA-4 in tumor digests following Nivolumab treatment (Figure 4f). For these markers, limited differences were observed in PBMCs (Supplementary Figure 3). Interestingly, T-cells co-expressing the three inhibitory molecules PD-1, TIGIT and LAG-3, were significantly increased in tumors from NIVO patients (Figure 4g). This demonstrated more differentiated intratumoral T-cells from the NIVO patients compared to control patients. Additionally, it suggests a compensatory upregulation of other inhibitory molecules, especially TIGIT, when PD-1 blocking takes place in GBM. Finally, the level of regulatory T-cells (Tregs) was low in tissue from controls, but highly heterogeneous

between NIVO patients (Figure 4h), indicating an induced anti-inflammatory TME after Nivolumab administration for a fraction of the patients.

Intratumoral gene expression analysis suggests increased immune infiltration to relapsed GBM tumors

Transcriptomic data obtained from the recurrent tumor samples were compared between NIVO and control group to investigate potential changes in the TME. By differential expression analysis (DEA) we found 1,716 differentially overexpressed genes and 260 genes which were differential under-expressed in the NIVO patients compared to control patients (Figure 5a).

The most significantly overexpressed genes were related to cancer progression (*MT-RNR1*, *SNOR7A*, *MIR663B*, *MIR6087*, *FGG*, *FGA*, *HMGCS2*, *PIP*, *REG1A*) rather than being related to immune response induced by Nivolumab treatment. Nevertheless, genes related to inflammation including *FOXA* and *CXCL17*; and *FGFBP2*, a gene related to T-cell effector function, was significantly overexpressed (Figure 5a). An unsupervised clustering resulted in separation of the Nivolumab-treated patients compared to untreated controls (Figure 5b). Additionally, with gene set enrichment analysis (GSEA), the TGF- β pathway was found to be enriched in NIVO patients (Figure 5c). Overall, the transcriptomic data showed the same tendency as determined through the T-cell evaluation; Nivolumab influences the TME with a sign of T-cell activation and upregulation of (compensatory) inhibitory pathways, such as TGF- β . Phenotypical characteristics of T-cells could not be assessed in the total tumor mRNA, likely due to the low T-cell content.

We further evaluated if any transcriptional and proteomics difference could be observed by comparing the patient's primary tumor, resected 4-34 months before entering this study, and the tumors resected after recurrence either following Nivolumab treatment (the NIVO group), or surgery only (the control group). An unsupervised clustering based on differentially expressed genes comparing primary and recurrent tumor sample showed a tendency to a split between the two groups. However, the same trend was observed for both NIVO and control patients (Supplementary Figure 5a). The unsupervised clustering of NIVO patients, was additionally confirmed based on proteomics data (Supplementary Figure 6). Using a GSEA, the B-cell receptor signaling pathway, the T-cell receptor complex and T-cell selection was found to be enriched in recurrent tumors from both NIVO patients and control patients (Supplementary Figure 5b), suggesting this signature relates to tumor relapse rather than Nivolumab-treatment itself. In line, CD3 stained histological FFPE sections from primary and recurrent NIVO tumors showed that most patients

(12 out of 20) had more CD3+ cells (T-cells) in the recurrent tumor compared to their corresponding primary sample (Supplementary Figure 7).

Of interest, upregulations of the inhibitory molecule, TIM-3, within the tumor following Nivolumab treatment was observed in the proteomics analyses (Supplementary Figure 8), further supporting the observed Nivolumab-induced effect on T-cell phenotype.

Autologous tumor reactivity of cultured TILs

We tested the tumor-reactive capacity of expanded TILs using intracellular cytokine staining of TILs after co-culture with autologous tumor digest. Reactivity in REP TILs against autologous tumor digest was demonstrated in four Nivolumab-treated patients (NVB02, NVB05, NVB08, NVB10) out of 16 tested patients. REP TILs from patient NVB02 and NVB05 showed clear responses among both CD4+ and CD8+ T-cells. For patient NVB10, we detected a small response only among CD8+ T-cells in REP TILs (Figure 6a, Supplementary Figure 9 and 10a). Overall tumor reactivity ranged between 1.2-13.6% reactive CD8+ TILs and between 6.3-10.9 % reactive CD4+ TILs (Figure 6a). To assess whether T-cell reactivity could influence patient outcome, we evaluated the mOS and mPFS of the patients with reactive T-cells to 17.0 months and 9.3 months, respectively. These were numerically higher compared to the NIVO patients without tumor-reactive TILs, mOS of 12.8 months and mPFS of 4.3 months, respectively (Supplementary Figure 10b). However, the difference was not significant. Due to the small study cohort applicable to TIL reactivity analyses, the results warrant further studies.

Transcriptomics analyses were performed to investigate differences in the TME between patients with tumor-reactive TILs, and the rest of the surgical group within the Nivolumab-treated patients. The DEA showed 1,522 differentially expressed genes and the reactive patients defined the first cluster-split, showing a large difference between the TME in the reactive and non-reactive patients. Among the overexpressed genes we found in the patients with reactive TILs were; *TGFB1*, *CXCL13* and *IL31RA*, which can all be related to inflammation (Figure 6b). The cluster-split dividing reactive and non-reactive was additionally confirmed by proteomics data, where we identified 22 overlapping differentially expressed genes (Supplementary Figure 11). From a GSEA, we identified differential overexpression of the MHC class I (MHC-I) peptide presentation pathway in patients with reactive TILs (Figure 6c). Additionally, when assessing the T-cell characteristics, we find a tendency for higher frequency of T-cells expressing CD28, and the inhibitory receptor TIGIT in tumors from patients with reactive TILs compared to the remaining NIVO patients. We also found significantly higher frequency of Tregs among CD4+ T-cells in the reactive

patients (Supplementary Figure 10c). In summary, the TME of these patients has a different gene-expression profile than the remaining NIVO patients, and an expression suggesting stronger T-cell activation and antigen presentation.

Neoantigen-reactive T-cells (NARTs) in PBMCs and TILs

To determine if neoepitopes could be targets for tumor cell recognition by T-cells in patients with tumor-reactive TILs, we screen for the presence of such neoantigen-reactive T-cells (NART) in both TILs and PBMCs, during treatment. Neoepitopes were predicted from the DNA exome and RNA sequencing from the primary and recurrent tumors. We screened PBMCs, YTILs and REP TILs for CD8+ T-cell recognition of neoepitopes using this personalized library of predicted neoepitopes and a pool of virus-derived epitopes, selected based on the patients HLA profile, to determine the level of virus antigen reactive CD8+ T-cells (VARTs) as a comparator. The screening was conducted using fluorescent and DNA barcode-labelled peptide-bound MHC-I multimers (pMHC), allowing pooling of 134-183 neoepitope pMHC multimers (PE labeled) and 3-16 virus-derived pMHC multimers (APC labeled) per sample (Figure 7a). We identified NART populations against 2-6 neoepitope-MHC per patient in PBMCs and/or TILs (Figure 7b, Supplementary Figure 12). The total number of responses across all evaluated patients are shown in Figure 7c, and the sum of estimated frequencies of NARTs and VARTs is shown in Figure 7d, both for each blood sample and for the TILs. When looking at the dynamics of the number of responses towards neoantigens, there was a trend for increase after Nivolumab treatment (week 3) for patient NVB02 and NVB05, which hereafter persist. The same pattern was observed for sum of estimated frequencies at week 3 and week 8, especially for NVB02. Neoantigen responses were only found at baseline and at week 8 in PBMCs from NVB10. However, the number and size of responses appears to increase at week 8. Neoepitope responses were only detected in TILs from NVB02 and NVB05, where both the number of responses, but also the estimated frequencies are increased in REP TILs compared to YTILs, most dominant in TILs from NVB02. The number of responses towards virus peptides in PBMCs remained relatively consistent throughout the treatment period, as did the sum of frequency of VARTs. All specificities were confirmed by a 14 day-patient-specific peptide stimulation of PBMCs (Supplementary Figure 13).

In summary, we screened for NARTs in YTILs, REP TILs and PBMCs. We found NARTs in TILs from NVB02 and NVB05. This coincides with NVB02 and NVB05 having the highest frequencies of reactive CD8+ TILs upon tumor challenge, while NVB10 had a relatively low CD8+ TIL response and NVB08 had no CD8+ TIL response (Figure 6a).

1 We further observed that the patients with tumor-reactive CD8+ TILs (NVB02, NVB05, NVB10) were
2 among the patients with the highest proportional overlap of mutations when comparing primary and
3 recurrent tumor (Supplementary Figure 14a). Furthermore, we observed a tendency of enrichment
4 ($p=0.06$, proportion z-test) of immunogenic neoepitopes, which was predicted from both primary and
5 recurrent tumor (4.3%), compared to immunogenic neoepitopes only predicted from one of the tumor
6 resection time points (1.6%) (Supplementary Figure 14b). Interestingly, we observed three neoepitopes
7 recognized by NARTs (LLILGIYST-A0201, LARVLVTLL-B5101, RVLVTLLIL-C0102), which originated from the
8 same frameshift mutation from the gene; *NF1* (Supplementary Figure 14c), suggesting extraordinary
9 immunogenicity of this genetic alterations, which opens a possibility to explore this further as a potential
10 shared neoantigen source. Patient NVB05 was the only patient with an *NF1* mutation among the four
11 screened patients.

Discussion

We present a translational phase 2 clinical study where we treated patients with recurrent GBM patients with Nivolumab and Bevacizumab every two weeks until progression, death or intolerable toxicity. We have shown that it was feasible and safe to use Nivolumab and Bevacizumab in this setting, but we could not demonstrate any direct benefit of Nivolumab combined with Bevacizumab on PFS or OS, when compared to historical control. But observed few patients who unexpectedly, based on existing clinical parameters, became long-term survivors. This study additionally offered a unique opportunity to explore the immune infiltration to GBM tumors, and the potential impact of Nivolumab treatment on the immune landscape.

Researchers are still in the early stages of understanding the immune system of the brain, and very little is known about the peripheral immune cells' role in the brain. We examined intratumoral T-cells in patients with recurrent glioblastoma, by evaluating the cellular impact of Nivolumab (aPD-1) treatment. Moreover, we studied the long-term effect of Nivolumab and Bevacizumab (aVEGF) treatment on peripheral T-cells in patients who did (surgical group) and did not (non-surgical group) receive resection of their recurrent tumor.

We confirmed the presence of Nivolumab in blood and importantly also in the tumor tissue. To our knowledge, it has not yet been demonstrated that Nivolumab can enter the TME of brain cancers. It can be questioned whether Nivolumab have entered as free immunoglobulins or bound to T-cells. The BBB strongly regulates passage of large molecules and cells into the brain tissue through tight junction ¹³. However, it has also been shown that the BBB in GBM can be disrupted and become more permeable in these tight junctions, which support both scenarios ^{14,15}. We found that PD-1 molecules on all intratumoral T-cells were saturated by Nivolumab in unrested digest, this also included tissue-resident T-cell within tumor tissue. This implies that Nivolumab can penetrate the tumor as free immunoglobulins. Previously, *Osa et al.* showed that, when Nivolumab-pretreated T-cells were cultured in Nivolumab free medium for more than 24 hours, the Nivolumab bound to the T-cells were lost. Moreover, they also showed that decreased concentrations of Nivolumab in plasma correlated with drop in level of Nivolumab-bound T-cells in blood from patients with non-small cell lung cancer ²⁵. Considering the findings of *Osa et al.*, our results indicate that Nivolumab has been in excess in the TME as intratumoral T-cells were saturated by Nivolumab, which further support that Nivolumab can enter the GBM microenvironment as an immunoglobulin alone.

We found that Nivolumab treatment affected T-cell phenotypical characteristics, both in the tumor and in the periphery, and moreover we could observe an effect on the TME based on RNA sequencing of tumor tissue. Firstly, intratumoral T-cells had higher expression level of the chemokine receptors CD183 and CD195 following Nivolumab administration. It has previously been shown that T-cells co-expressing CD195 and CD183 can be detected in CSF and PBMCs of multiple sclerosis patients and other cases of neurological inflammation, but not in non-inflammatory neurological diseases ^{23,24}. To this end, our results indicate that a recruitment to the GBM tumor is boosted due to increased inflammation caused by Nivolumab treatment. Additionally, we found that Nivolumab-treated patients who retrained their tumor had higher frequencies of CD8+ T-cells expressing CD183 and CD195 in the blood compared to the tumor resected group. This observation supports that peripheral T-cells are actively being recruited to the brain due to neurological inflammation, also in a cancer setting. However, it should be further investigated by analyzing the level of CNS homing T-cells in the blood as well as in the CSF of the two patient groups. Furthermore, intratumoral T-cells of NIVO patients were found to have higher frequency of T-cells expressing markers of activation, CD39 and CD137, compared to control patients. CD39 co-expressed with the tissue-resident marker CD103 has previously been identified as a unique CD8+ T-cell population within the TME, which were then found to be enriched for tumor-reactive T-cells as well as correlating with longer survival in patients with head and neck cancer ²⁶. We demonstrated increased frequencies of CD39+ tissue-resident CD8+ T-cells in tumor digest from Nivolumab-treated patients compared to control patients. While CD39 are lately - and more persistently expressed upon T-cell activation, CD137 expression both increases and attenuates quickly after T-cell antigen recognition and stimulation ²⁷⁻³¹. We found a trend for increased expression of CD137 on tissue-resident CD8+ T-cells after Nivolumab treatment. Such cell were present at low frequencies, which could be explained by the transient expression kinetics of CD137 ²⁸. Thus, collectively PD-1- blocking have most likely led to an increased TCR activation of intratumoral T-cells, also supported by overexpression of *FGFBP2*, a gene related to T-cell cytotoxicity ^{32,33}. Furthermore, the co-stimulatory molecule, CD28 were expressed on the majority of intratumoral T-cells, though there was a substantial diversity in the frequency of CD28+ CD8+ T-cells within the Nivolumab-exposed tumors. Previous studies show that CD28+ T-cells respond well to PD-1 therapy and that loss of CD28 on CD8+ T-cells is a marker for unresponsive patients ^{34,35}. We observed that patients with high frequency of CD28+ CD8+ T-cells in the tumor had a longer PFS and OS after recurrence. Interestingly, this was only evident for Nivolumab-treated patients and not controls, why CD28 frequency among effector T-cells could indicate a successful response to treatment. In addition, PD-1 acts primarily by inhibiting the co-stimulatory signal through CD28, rather than TCR signaling ³⁶. We found that CD28 expression was

1 significantly higher on intratumoral T-cells following Nivolumab administration. Thus, it could be
2 speculated whether Nivolumab treatment not only results in blocking of the inhibitory signaling but also
3 allow T-cells to increase expression of CD28 and unleash co-stimulation. Co-stimulation and activation
4 would lead to expansion and proliferation of tumor specific T-cell clones, supported by higher frequency
5 of Ki67+ intratumoral T-cells within Nivolumab-treated patients.

6 Even though we find an upregulation of activation and proliferation within intratumoral T-cells following
7 Nivolumab treatment, an anti-inflammatory TME appeared to be boosted, perhaps as feedback to an
8 increased immune activation caused by PD-1 blocking. Analysis of transcriptomic data showed an
9 enrichment of the TGF- β pathway in the TME of Nivolumab-treated patients. CD39 expression is known
10 to be upregulated in the presence of TGF- β ^{26,37,38}. In addition, CD39 have also been described to have a
11 regulatory function, as it together with CD73 generates adenosine from ATP, which also contributes to an
12 anti-inflammatory TME ³⁹. Interestingly, PD-1 expression was measured in lower frequencies of
13 intratumoral CD8+ T-cells in Nivolumab-treated patients compared to controls. A similar effect of
14 Nivolumab was detected in blood, with a decrease in the frequency of T-cells expressing PD-1 after
15 Nivolumab administration (Figure 4b and 4c). This could be due to endocytosis of the receptor after
16 Nivolumab binding, as the case is for other receptors after engagement of their target ^{40,41}, but it needs
17 to be evaluated further. Importantly, a compensatory upregulation of additional inhibitory molecules,
18 including LAG-3, TIM-3, CTLA-3 and TIGIT, were detected within intratumoral T-cells following Nivolumab
19 and thus potentially contribute to drug resistance ⁴². In particular, TIGIT was expressed on a larger fraction
20 of T-cells, and could therefore be a relevant co-target as has previously been suggested ^{43,44}. Altogether
21 these results imply that Nivolumab have reached the tumor tissue and have led to T-cell activation and
22 differentiation, as well as influenced the TME, even within a short time span of seven days.

23 Next, we were able to detect tumor reactivity in REP TILs from 25% (4 out of 16) of Nivolumab-treated
24 patients. Interestingly, we found a clear difference in the TME landscape of patients with tumor-reactive
25 TILs compared to the remaining Nivolumab-treated patients based on transcriptomic data. Specifically,
26 we found a gene set enrichment of the pathway involved in antigen processing and presentation on MHC-
27 I. This could indicate an ongoing presentation of potential immunogenic neoepitopes to T-cells within the
28 TME of these patients, providing a potential for CD8+ T-cell-mediated cancer-cell killing ^{45,46}. We therefore
29 examined the tumor specificity of the reactive TILs further by screening PBMCs and TILs for the presence
30 of neoantigen-reactive CD8 T-cells (NARTs). We were able to detect NARTs in TILs from two patients which
31 matched with the patients who showed the highest reactivity against tumor. Interestingly, the NARTs

1 detected in these patients (NVB02 and NVB05) were specific to neoantigens found in both the primary
2 and recurrent tumor, potentially representing clonal mutations. In fact, we detected three immunogenic
3 neoepitopes from patient NVB05 derived from a frameshift mutation in *NF1*. Mutations in the *NF1* gene
4 has been reported in 13-14% of GBM, hereof 78% consisting of frameshifts ⁴⁷. Additionally, NF1 mutations
5 has been described to be related to high T-cell infiltration in gliomas ⁴⁸. Therefore, such mutations could
6 be of interest as potential biomarker for use of immunotherapy treatment. In line, the T-cell infiltration
7 and quality of neoantigens, and thereby the potential to induce a potent tumor specific T-cell response
8 has previously been correlated with longer survival for GBM patients ⁴⁹. Our results support this with a
9 higher PFS and OS after recurrence for patients with tumor-reactive TILs, compared to the remaining
10 patients in the Nivolumab-treated group, though it was not significant in this small patient group.
11 Personalized neoantigen vaccines have been tested in order to induce and boost the NART repertoire in
12 GBM patients, but despite tumor infiltration of vaccine-induced NARTs, immune suppressive factors
13 diminished the immune response ^{50,51}. In line with this, we observed in TIL-reactive patients, enhanced
14 expression of the inhibitory molecule, TIGIT, and higher frequency of Tregs among CD8+ and CD4+ T-cells,
15 respectively, along with overexpression of *TGFB1*. This supports the need for combination therapy to
16 overcome such compensatory immune inhibition and improve treatment outcome for these patients.
17 Additionally, we report an enrichment of genes related to lymphocytes pathway in recurrent tumors
18 compared to the primary tumors, along with a higher detection of T-cells in histological FFPE section of
19 recurrent Nivolumab treated tumors compared to paired primary tumors. This could imply that there was
20 an increased infiltration of lymphocytes in recurrent tumors compared to primary tumors, underpinning
21 the potential relevance of immunotherapy in the recurrent setting.

22 Finally, an increasing number of observations suggests that the peripheral immune system play a role in
23 the immunosurveillance of the brain ⁶⁻⁹. Importantly, we detected the same NART populations in both
24 blood and tumor samples, confirming an interaction between the brain tumor and the peripheral immune
25 system. This is additionally supported by a study identifying GBM specific NARTs in blood ⁵². Moreover,
26 we find that both the number and the sum of estimated frequency of the NARTs increased after
27 Nivolumab treatment. This aligns with previous observations from other cancer cohorts, where therapy
28 targeting the PD-1/PD-L1 axis, resulted in a boost of the number NARTs in PBMC shortly after treatment
29 initiation ⁵³.

30 In conclusion, we reported that Nivolumab can reach GBM tumors. After only seven days, an effect could
31 be observed on both intratumoral T-cells and in the gene expressing profile of the TME. We found that

1 intratumoral T-cells had an increased activated, but also a differentiated phenotype, and the TME showed
2 both indication of cytotoxic response, but also an immunosuppressive profile. Furthermore, we found
3 tumor-reactive TILs from four Nivolumab-treated patients, where NARTs were also identified. These
4 patients had longer PFS and OS and high frequencies of CD28+ CD8+ T-cells, however anti-inflammatory
5 factors were also induced. Importantly, NARTs could be detected in PBMC and appeared to be boosted
6 after Nivolumab administration. Altogether, to improve immunotherapies for GBM we need to consider
7 the complexity of the tumor and the resistance mechanism induced after PD-1 blockade. It is likely that
8 some patients will benefit from this treatment, why it is important to identify the characteristics
9 associated to clinical responses, as well as offering selected patients a combination therapy to overcome
10 the adaptable resistance mechanisms.

Acknowledgements

We thank all patients who donated material that was used in this study; the funding that supported this research; Group leader, MD, PhD M. Donia and MD and M. Presti for invaluable support and critical review of the manuscript and assistant with laboratory work; PhD T. Tamhane and A. D. E. G. Burkal for production of MHC class I monomers; B. Rotbøl and A.F. Løye for technical assistance handling the flow cytometry instruments and samples; O. S. G. Heiede for technical assistance with flow cytometry analysis.

Author contributions

SKS study design, performing experiments, analysis and interpretation of data, generation of figures and tables, statistical analysis, writing manuscript; SM study design, collection of patient samples, performing experiments, analysis of data, generation of figures and tables, writing manuscript; AD study designed, performing experiments, data analysis; AB prediction of neoepitopes, bioinformatics analyses and generation of figures; SH bioinformatics analyses and generation figures; FM study designed and performing experiments, analysis of data; MM study designed and performing experiments, analysis of data; JSR study supervision and data discussion; CWY providing WES- and RNA-seq data; HSP conceiving study concept, patient contact, funding, study supervision and data discussion; BH conceiving study concept, patient contact, funding, study supervision, data discussion; IMS conceiving study concept, funding, study supervision, data discussion; UL conceiving study concept, patient contact, study supervision, data discussion, funding support; SRH conceiving study concept, study supervision, data discussion, funding, writing manuscript. IJC: critical review of data and managing statistical design and analyses. VP: Support, managing and evaluation of histological (FFPE) sections. BWK: Support, managing and evaluation of histological (FFPE) sections as well as funding for pathological analyses.

Conflicts of interest

Nivolumab was provided by Bristol-Meyer Squibb. Bristol-Meyer Squibb did not exert any influence on the study and did not provide financial support for the study. SRH is the cofounder of PokeAcell and is the coinventor of patents WO2015185067 (Determining antigen recognition through barcoding of MHC multimers) and WO2015188839 (General detection and isolation of specific cells by binding of labeled molecules) for the barcoded MHC technology that is licensed to Immudex. IMS has received grants from

1 or signed contracts with Bristol-Myers Squibb, Adaptimmune, IO Biotech, Lytix biopharma, TILT
2 Biotherapeutics, and Enara Bio; has received consulting fees from MSD, IO Biotech, Novartis, Pierre Fabre,
3 Novo Nordisk, and TILT Biotherapeutics; has received honoraria for lectures, presentations, or educational
4 events from MSD, Novartis, Sanofi Aventis, Pierre Fabre, Bristol-Myers Squibb, IO Biotech, TILT
5 Biotherapeutics, Novo Nordisk, and Takeda; has received support for attending meetings and/or travel
6 from MSD; owns IO Biotech stocks.

Methods and Materials

Trial design

CA209-9UP is an open label phase 2 clinical trial, designed as a trial in a real-life setting to evaluate treatment of recurrent glioblastoma (GBM) with Nivolumab and Bevacizumab under conditions close to routine practice (NCT03890952). In this study Bristol-Meyer Squibb sponsored Nivolumab. Patients had at primary diagnosis received Stupp's regimen¹. Patients were treated at Rigshospitalet, Copenhagen University Hospital but the inclusion was open nationally upon transfer. In total 44 patients (4 screen failures) were included in a surgical group (N=20) and non-surgical group (N=20) depending on the possibility of salvage neurosurgical resection (Figure 1a, Supplementary Figure 1). All patients received 240mg Nivolumab and 10mg/kg Bevacizumab every two weeks. The surgical group also received 240mg Nivolumab approximately seven days prior surgery. In total 44 patients were included by January 2021, follow-up was ended May 2022. End points were translational research, safety, and efficacy. The trial was approved by the Danish Ethical Committee (EudraCT 2017-003925-13), written consents were obtained with the possibility to withdraw consent at any time. Age at diagnosis, performance status and multifocal disease at inclusion were registered. Extent of surgical resection was extracted from the operation note. Corticosteroid use was found in the record, medicine registry or operation note. IDH1/IDH2 mutations were investigated by immunohistochemistry and next-generation sequencing. Cut-off value for O-6-methylguanine-DNA methyltransferase (MGMT status); methylated/un-methylated was 10%. Additional inclusion and exclusion criteria are listed in Supplementary Table 5. Additionally, control patients (N=10) with recurrent glioblastoma undergoing neurosurgical resection were included and donated fresh tumor tissue. The controls did not receive Nivolumab or Bevacizumab in the recurrent setting. We used real world data as controls from our GBM database on patients from Rigshospitalet Copenhagen, we found 156 patients treated with Irinotecan and Bevacizumab at recurrent setting from 2006-2014. Gender was equally distributed, ages ranged from 23-79 years and the median age was 58 years. Of the 156 patients, 81 patients had salvage resection while 75 patients had none. Clinical data from these patients were used as historical controls.

Statistical analyses and considerations of clinical results

The Kaplan-Meier method was used to estimate survival probabilities for overall survival (OS) as well as progression-free survival (PFS) for patients stratified by group with log rank statistics. Comparison of the patients in the trial to the historical control was weighted using propensity scores based on age, gender, corticosteroid use, multifocal disease, MGMT status and extent of resection. Separate analyses were done

for those undergoing reoperation or not. Results were presented with 95% confidence limits and the significance level was 5%. Calculations were done using SAS (v9.4, Cary, N.C., USA). Multivariate analysis was performed using the Cox proportional hazards model with covariates; treatment group, gender, age per 10 years, MGMT status, corticosteroid use.

Patient material

RNA/DNA extraction from tumor tissue or blood

Paired samples from primary and recurrent tumors were available from the surgical group; Recurrent tumor samples were collected and stored in RNeasy Lysis Buffer (Qiagen) immediately after resection. Archival tissue from autologous primary tumor was available as fresh frozen tissue or formalin fixed paraffin embedded (FFPE) tissue. Blood samples for germline DNA were collected in Streck- and EDTA vials. DNA and RNA were extracted from fresh frozen tissue by AllPrep RNA/DNA/Protein Mini Kit (Qiagen). RNA was further DNase treated with RNeasy mini kit (Qiagen). DNA and RNA were extracted from FFPE slides by GeneRead DNA FFPE kit (Qiagen) and Agencourt FormaPure Reagent Kit (Beckman Coulter), respectively. DNA from blood for germline whole exome sequencing (WES) was extracted by ReliaPrep Large Volume HT gDNA isolation system (Promega). Manufacturers' instructions were followed for all kits. Bioanalyzer 2100 with the 6000 RNA Nano and Pico Assay was used to evaluate the RNA quality. RNA was quantified using DeNovix Spectrophotometer. DNA was quantified using Qubit Fluorometric Quantification (Thermo Fisher Scientific). Library preparation for WES was done by SureSelect Clinical Research Exome (Agilent). Library preparation for RNAseq was performed using TruSeq Stranded total RNA kit (Illumina). All sequencing was performed on Illumina NovaSeq 6000 (Illumina).

Peripheral blood mononuclear cells (PBMCs)

Peripheral blood samples were collected from patients at several time points (Figure 1a); baseline (day 0, prior to treatment), after 8 weeks and 16 weeks. One additional blood sample was collected 3 weeks after Nivolumab administration in the surgical group – two weeks after surgery. Peripheral blood mononuclear cells (PBMCs) were isolated using Lymphoprep density gradient (Takeda) and cryopreserved in 10% DMSO (Herlev Hospital Pharmacy) and 90% human serum (Sigma-Aldrich/Merck KGaA) using controlled-rate freezing (Cool-Cells, Biocision) in -80 °C, and later stored in -140 °C (Figure 1a).

Tumor infiltrating lymphocyte in vitro expansion

Minimally-expanded Young Tumor infiltrating lymphocytes (YTILs) were expanded from resected tumor tissue. Tumor tissue was cut into 1-3 mm³ fragments and plated in wells of a 24 well-plate with 2 mL

complete medium consisting of 90% RPMI-1640 plus GlutaMAX and 25 mM HEPES (Gibco, Thermo Fisher Scientific), 10% heat-inactivated human AB serum (Sigma-Aldrich/Merck KGaA, Darmstadt, Germany), 100 U/mL penicillin, 100 µg/mL streptomycin (Gibco, Thermo Fisher Scientific, Waltham, MA), 1.25 µg/mL Amphotericin B (Fungizone®, Bristol-Myers-Squibb), and 6000 IU/mL of rhIL-2 (Proleukin®, Novartis). Plates were incubated at 37 °C with 5% CO₂ and were inspected every other day from day five to investigate extrusion and proliferation of lymphocytes. Half of the medium was replaced with fresh complete medium every other day after day 5. Cells were split when needed, harvested after 3-6 weeks and cryopreserved as described above.^{55,56}

Rapid expanded TILs (REP TILs) were expanded YTILs (just harvested or thawed). When biopsies were sparse, REP TILs were prioritized over young TILs due to higher success rate in production of REP TILs than YTILs. Frozen YTILs were thawed and cultured in complete media for 48 hours prior rapid expansion. During rapid expansion, 100000 YTILs were co-cultured with feeder cells and 30ng/mL anti-CD3 (clone OKT-3, Miltenyi Biotec) in 10mL complete medium and 10mL rapid expansion medium, which consisted of AIM-V (Thermo Fisher Scientific) and Fungizone® 1.25 µg/ml supplemented with 6000 IU rhIL-2/ml in T25 flasks (Thermo Fischer Scientific). Feeder cells (PBMCs) from minimum six donors were thawed and irradiated by 40 Gy (Gammacell 3000 Elan, MDS Nordion). REP cultures were incubated at 37 °C with 5% CO₂ for 5 days. On day 5 of the rapid expansion, half of the medium was replaced with 10mL of mixed medium (consisting of 1:1; complete medium:rapid expansion medium). According to growth, the cultures were moved to larger flasks and rapid expansion medium was added over the next 9 days. At day 14+1, REP TILs were harvested and cryopreserved as mentioned above.^{55,56}

Tumor digest (single cell suspension)

Fresh tumor samples from the operating theater were transported in medium (RPMI-1640+ GlutaMAX and 25mM HEPES) (Gibco, Thermo Fisher Scientific) supplemented with 100 U/mL penicillin and 100 µg/mL streptomycin (Pen Strep, Gibco, Thermo Fisher Scientific) on ice. The fresh tumor tissue was dissected under sterile conditions into fragments after the macroscopical vessels were removed. Tumor fragments were then placed in T80 flask with 25 mL of digesting medium consisting of 100 mL RPMI-1640 plus GlutaMAX and 25mM HEPES supplemented with 1% Pen/Strep, 1 mg/mL Collagenase (Cat No C5138-100MG, Sigma-Aldrich), 0.025 mg/mL Dornase alfa (Pulmozyme®, Genentech), and placed overnight on a magnetic stirrer at room temperature. After minimum of 18 hours the digested tumor fragments were filtered through 70 µM filter to obtain a single cell suspension. The single cells was cryopreserved as aforementioned.

Immunohistochemistry

Formaldehyde fixed paraffin embedded (FFPE) glioblastoma tissue from patients and controls were cut on a microtome (2 μ m). The 10 controls had pathologically verified GBM and used a maximum of 20 mg prednisolone, comparable to the inclusion criteria in the trial. Tissue sections were deparaffinized and subject to heat-induced epitope retrieval with either Cell Conditioner 1 for 84 minutes at 100°C (CD3, PD-1 and IgG4) or EnVision TRS low pH, 40 minutes at 97°C (PD-L1). Endogenous peroxidase activity was blocked. Incubation with CD3 Ready-To-Use (RTU) antibody (clone: 2GV6, Roche), PD-1 antibody (clone: MRQ22, Roche) diluted in EnVision FLEX Antibody Diluent K8006 and IgG4 antibody (clone: MRQ44, Cell Marque) diluted in the same diluent was done using the BenchMark ULTRA Platform (Ventana Medical Systems) with the OptiView DAB IHC Detection system (Roche Diagnostics). Incubation with PD-L1 RTU antibody (clone: 22C3, Dako) was done using the Dako Omnis Platform (Agilent Technologies) using the EnVision FLEX DAB+ Chromogen (Dako Omnis) detection system. Nuclei were counterstained with hematoxylin. Human tonsils were used as controls and stained as above. Slides were evaluated by conventional microscopy and reviewed by neuropathologist co-author BWK. Slides were digitalized using the NanoZoomer XR digital image scanner (Hamamatsu, Japan).

Phenotyping by flow cytometry

Cryopreserved PBMCs, YTILs, REP TILs and tumor digest were thawed and washed once in RPMI 1640 Medium with 10% fetal bovine serum (FBS) for cellular staining. Tumor digest was thawed and rested overnight in X-vivo 15 (Lonza) with 5% heat-inactivated sterile filtered human serum (HS, Sigma-Aldrich) to regain surface-marker expression after enzymatic digestion. PBMCs, YTILs and REP TILs were thawed immediately before staining. PBMC and tumor digest were washed twice in PBS with 2% FBS (FACS buffer), stained with a panel of fluorochrome conjugated antibodies for surface markers (Supplementary Table 6) for 30 minutes (dark, 4 °C), and cells were washed twice in FACS buffer. For staining of intracellular (ICS) marker in panel B, C and D we used the eBioscience™ Foxp3/Transcription Factor Staining Buffer Set (Invitrogen) following manufacturer's protocol. Fixation/permeabilization working solution was added to surface stained PBMCs and - tumor digest and incubated overnight (dark, 4 °C). Cells were washed twice in 1X Permeabilization Buffer and antibodies for intracellular markers were added and cells were stained for 30 minutes and hereafter washed twice with 1X Permeabilization Buffer. PBMCs and digest stained with panel A (surface markers) were fixated in 1% PFA. Samples were resuspended in FACS buffer and acquired on LSRFortessa (BD bioscience).

Analysis of flow cytometry data

Tumor digest contained much debris and lymphocyte counts varied between patients. Samples with less than 30 events in the parent populations (CD4⁺ T-cells or CD8⁺ T-cells) were not included in the analysis. Number of events in parent population per patient samples are shown in Supplementary Figure 15a. Flow cytometry data was analyzed in FlowJo v10.8.1. Manual gating was performed as depicted in Supplementary Figure 15b.

In order to compare expression level of markers analyzed by flow cytometry, adjusted MFI fold change was calculated from MFI of positive population (MFI_{pos}) and MFI of negative population (MFI_{neg}) for each of the markers of interest as followed;

$$MFI \text{ fold change} = \frac{MFI_{pos} + 1000}{MFI_{neg} + 1000}$$

As MFI_{neg} could have a negative value, we added 1000 to each MFI_{pos} and MFI_{neg} and hereafter calculated the fold change MFI based on adjusted numbers. Samples with parent population (CD4⁺ T-cells or CD8⁺ T-cells) less than 30 events were not included in the analysis. MFI fold change was set to 1 for samples with a positive population less than 10 events.

Unpaired t-test was used to compare means of two groups and performed with a 95% confidence interval.

* = p<0.05, ** = p<0.01, *** = p<0.001, **** = p<0.0001.

TIL Reactivity Assay

YTILs and REP TILs were tested for reactivity against autologous tumor digest with cytokine intracellular staining. TILs were thawed in pulmozyme buffer (RPMI-1640+GlutaMAX and 25mM HEPES) (Gibco, Thermo Fisher Scientific) supplemented with 100 U/mL penicillin, and 100 µg/mL streptomycin (Pen/Strep, Gibco, Thermo Fisher Scientific), 0.5mL of Magnesium chloride (Herlev Hospital Pharmacy and 0.025 mg/mL dornase alfa (Pulmozyme®, Genentech)) washed and cultured in RPMI+ Pen/Strep+ 10% HS with a concentration of 2-4x10⁶ cells/mL. TILs were rested overnight at 37 °C, 5% CO₂. Tumor digests were thawed in transport medium and washed. Cells from tumor digests were counted and resuspended in RPMI-1640+ Pen/Strep+ 10% HS in a concentration of 2x10⁶ cells/mL. TILs were washed and resuspended in RPMI-1640+ Pen/Strep+ 10% HS in a concentration of 3x10⁶ cells/mL. TILs and digest T-cells were co-cultured in a ratio of 3:1 by adding 100µL TILs suspension and 50µL autologous tumor digest suspension in a sterile 96 well plate (Thermo Scientific). GolgiPlug (BD Biosciences), GolgiStop (BD Biosciences) and anti-CD107a (BD Biosciences) were added according to manufacturer's recommendations and RPMI-

1640+ Pen/Strep+ 10% HS was added up to a total volume of 200µL per well. TILs stimulated with PMA/ionomycin (25ng/0.5uM) (Sigma Aldrich/Sigma Aldrich) or 0.4uL Leukocyte Activating Cocktail (BD biosciences) were used as positive controls. TILs alone were used as negative controls. Melanoma tumor cell line without MHC-I and II expressions due to *B2M* or *CIITA* knockout by CRISPR-associated protein 9 (CAS9) was additionally used as negative controls, both previously described^{55,57}. The co-cultures were incubated for 8 hours in a humidified incubator 37°C with 5% CO₂ and then stained as described above (Supplementary Table 6, panel C or D). Stained cells were acquired on the LSRFortessa or NovoCyte Quanteon Flow Cytometer (Agilent, Santa Clara, CA) and analyzed with FlowJo 10.6.1 or 10.8.1.

9 Transcriptomics

10 Preprocessing of the RNA sequencing FASTQ files was done using trimming with TrimGalore 0.6.4⁵⁸ which
11 was combined with Cutadapt⁵⁹ and FastQC version 0.11.9⁶⁰. Kallisto Quant version 0.46.0⁶¹ was used to
12 align the trimmed reads to GRCh38⁶².

13 Proteomic analyses

14 *Sample preparation for mass spectrometry-based*

15 Samples were processed by Qiagen© AllPrep DNA/RNA/Protein Mini Kit for protein purification. The final
16 flow-through containing the proteins was processed through acetone precipitation as previously
17 described⁶³. The resulting protein pellet was re-suspended in 200 µl, 8 M urea, in Tris-HCl (pH 8.0).
18 Supplemented with PhosSTOP (Roche) and Complete Protease Inhibitor (Sigma Aldrich), following the
19 manufacturers' instructions. The pellet was completely dissolved by pipetting and sonication (Bioruptor®,
20 Diagenode; 5 times 30 seconds on and 30 seconds off cycles). Protein concentrations were determined
21 and protein solutions were reduced and alkylated as described, followed by tryptic digest and peptide
22 clean up on two 14-gauge styrene divinylbenzene reverse phase sulfonate StageTip plugs using a
23 previously described protocol^{63,64}. Clean peptides were resuspended in 10 µL 0.1 % formic acid and
24 analyzed on a NanoDrop™ for their concentrations as before.

25 *Mass spectrometry analyses*

26 A total of 200 ng clean peptides were loaded on C18 Evotips (EvoSep) following manufacturer's protocol.
27 Briefly, tips were wetted in isopropanol for 10 seconds, and then activated with 20 µL 100 % acetonitrile
28 with 1 % formic acid. Evotips were cleared by one minute centrifugation at 800 round centrifugal force
29 (rcf) and again wetted in isopropanol for 10 seconds. Then the Evotips were conditioned with 20 µL of 0.1

% formic acid and cleared for one minute at 800 rcf before 200 ng of samples were loaded and spun down (800 rcf for one minute). We loaded a total of 300 ng of de-salted peptides per sample on each tip. Tips were then washed ones with 20 μ L of 0.1 % formic acid and centrifuged at 800 rcf for one minute, before stored with 100 μ L of 0.1% formic acid on the tips and plenty of 0.1 % formic acid in the Evotip box to prevent drying. The charged tips were loaded on an EvoSep One liquid chromatographer (EvoSep) and injected at a rate of 30 samples per day, i.e., with a 44-minute gradient. Samples were analyzed on a TimsTOF Pro (Bruker) using diaPASEF acquisition mode. The column used was commercially pre-packed with 1.5 μ m C18-beads (PepSep) with the following dimensions: 15 cm \times 150 μ m inner diameter. Column was heated to 40°C during the runs. The original dia-PASEF method in Meier et al.⁶⁵ Mass spectrometry diaPASEF raw files were searched with DIA-NN software (version 1.8). Samples were searched against the human FAST files (9606), which were in silico digested for library free searches and library generation. Missed cleavages were set to 1, and number of allowed variable modifications to 2. N-terminal methionine excision, carbamidomethylation of cysteines, oxidation of methionine and N-terminal acetylation were selected as modifications. Peptide lengths were allowed within, and including, 7 to 30 amino acid residues. Precursor charge range was set to 2 to 4, precursor m/z range from 100 to 1700, and fragment ion m/z range from 200 to 1800. Mass accuracy and MS1 accuracy were both set to 15.0, match between runs were enabled and likely interferences were removed. Data was re-searched in a second pass using the on-the-fly generated spectral library. For more details see DOI: <https://doi.org/10.1101/2023.05.12.540582>⁶³. Data was log2-transformed and median-MAD (median absolute deviation) normalized (robust z-scores) before bioinformatical analyses.

Differential expression analysis

Differential expression analysis (DEA) for proteomics and transcriptomics was performed with DeSeq2 version 1.30.1⁶⁶ and the results with genes and log-fold change were used as input to a Gene Set Enrichment Analysis (GSEA) with clusterprofiler packages from R version 4.2.2⁶⁷ and both the Gene Ontology database (GO) and Kyoto encyclopedia of genes and genomes (KEGG) database was applied. Complexity heatmap version 2.10⁶⁸ was used for the heatmap and enrich figures were made with geasqplot2 from enrichplot⁶⁹.

Detection of Neoantigen-reactive T-cells in PBMCs and TILs

Neoantigens were predicted with the following pipeline; The mutations are detected by the GATK4 best practice⁷⁰. Firstly, the WES reads were trimmed using TrimGalore 0.6.4⁵⁸ combined with Cutadapt⁵⁹ and

FastQC 0.11.9⁶⁰ with a minimum length of 50 bp, and else default settings. The trimmed reads were aligned to the human reference genome, GRCh38⁶² using BWA-MEM 0.7.16a⁷¹ followed by the pre-processing steps including MarkDuplicate and base re-calibrator⁷⁰. Somatic variant calling called using MuTect2⁷² with filtering of panel of normal (PON) and contamination filter from GTAK best practice. MuPexi⁷³ were used to predict neoepitope candidate which were filtered by the expression of the corresponding gene obtained from kaillisto version 0.46.0⁶¹ and the binding to the corresponding HLA-allele predicted with NetMHCpan 4.1⁷⁴. The patient specific HLA-allele were typed used Razers3 (version 3.4)⁷⁵ followed by OptiType version 1.2⁷⁶. The criteria for selecting neoepitope candidates were expression level ≥ 0.1 TPM and then top 100 of the best EL%Rank to the HLA allele but only including HLA binders. Neoantigens were predicted for both primary and recurrent tumor.

PBMCs, YTILs and REP TILs were screened neoantigen-reactive CD8 T-cells (NARTs) and virus antigen reactive T-cells (VARTs) using DNA barcode-labelled peptide-MHC-I multimers ⁷⁷. In short DNA barcode-labelled peptide-MHC-I multimers are assembled, so each DNA barcode is specific for each pMHC in the neoantigen panel. The multimers are built on a dextran backbone, which is labelled by a fluorochrome (NARTs: PE, VARTs: APC). Patient samples were stained with a patient specific pool of pMHC multimers, together with CD8 and CD3 antibodies (Supplementary Table 6). PE and APC labelled CD8+ T-cell are hereafter sorted by Fluorescence activating cell sorting (FACS) on FACSaria (BD). DNA barcodes in the sorted cells were hereafter amplified by PCR. A baseline sample from the multimer pool was also amplified as a reference. PCR products were sequenced by Primbio and sequencing results were hereafter analysed in Barracoda ⁷⁷. Output files from Barracoda included information on the fold change of enriched DNA barcodes in the sorted samples compared to the baseline and whether the enrichment is significant. A fold change (log2) over 2 and $p < 0.001$ was set as threshold for a significantly enriched DNA barcode, wherefrom the T-cell recognition of pMHC was annotated.

Verification peptide reactivity

Peptides detected by NARTs was verified by peptide specific expansion of patient PBMCs. PBMCs were co-cultured with a pool of reactive peptides for 14 days. PBMCs were cultured in X-vivo (Lonza) with 5% human serum. Peptides were added at day 0 with a concentration of 10 $\mu\text{g/ml}$ per peptide. PBMCs were additionally stimulated with 40 IU/ml IL-2, and 0.5 $\mu\text{g/ml}$ purified anti-CD28 (BD, clone: CD28.2). Medium with IL-2 was changed twice per week. PBMCs expanded with peptides were hereafter stained with single tetramers to validate the pMHC specificity of the given T-cell cultures. Each tetramer was fluorochrome labelled with both PE and APC. PBMC samples was analysed by LSRFortessa (BD) and gated in FlowJo v10.

References

1. Stupp, R. *et al.* Radiotherapy plus Concomitant and Adjuvant Temozolomide for Glioblastoma. *N. Engl. J. Med.* **352**, 987–996 (2005).
2. Wen, P. Y. *et al.* Glioblastoma in adults: a Society for Neuro-Oncology (SNO) and European Society of Neuro-Oncology (EANO) consensus review on current management and future directions. *Neuro. Oncol.* **22**, 1073 (2020).
3. Schalper, K. A. *et al.* Neoadjuvant nivolumab modifies the tumor immune microenvironment in resectable glioblastoma. *Nat. Med.* **25**, 470–476 (2019).
4. Arrieta, V. A. *et al.* ERK1/2 phosphorylation predicts survival following anti-PD-1 immunotherapy in recurrent glioblastoma. *Nat. cancer* **2**, 1372 (2021).
5. Medawar, P. B. Immunity to Homologous Grafted Skin. III. The Fate of Skin Homographs Transplanted to the Brain, to Subcutaneous Tissue, and to the Anterior Chamber of the Eye. *Br. J. Exp. Pathol.* **29**, 58 (1948).
6. Bartholomäus, I. *et al.* Effector T cell interactions with meningeal vascular structures in nascent autoimmune CNS lesions. *Nature* **462**, 94–98 (2009).
7. Louveau, A. *et al.* Structural and functional features of central nervous system lymphatic vessels. *Nature* **523**, 337–341 (2015).
8. Aspelund, A. *et al.* A dural lymphatic vascular system that drains brain interstitial fluid and macromolecules. *J. Exp. Med.* **212**, 991–999 (2015).
9. das Neves, S. P., Delivanoglou, N. & Da Mesquita, S. CNS-Draining Meningeal Lymphatic Vasculature: Roles, Conundrums and Future Challenges. *Front. Pharmacol.* **12**, (2021).
10. Nayak, L. *et al.* Randomized Phase II and Biomarker Study of Pembrolizumab plus Bevacizumab versus Pembrolizumab Alone for Patients with Recurrent Glioblastoma. *Clin. Cancer Res.* **27**, 1048–1057 (2021).
11. Reardon, D. A. *et al.* Treatment with pembrolizumab in programmed death ligand 1–positive recurrent glioblastoma: Results from the multicohort phase 1 KEYNOTE-028 trial. *Cancer* **127**, 1620–1629 (2021).

- 1 12. Larkin, J. *et al.* Five-Year Survival with Combined Nivolumab and Ipilimumab in Advanced
2 Melanoma. *N. Engl. J. Med.* **381**, 1535–1546 (2019).
- 3 13. Pluim, D. *et al.* Enzyme linked immunosorbent assay for the quantification of nivolumab and
4 pembrolizumab in human serum and cerebrospinal fluid. *J. Pharm. Biomed. Anal.* **164**, 128–134
5 (2019).
- 6 14. Liebner, S. *et al.* Claudin-1 and claudin-5 expression and tight junction morphology are altered in
7 blood vessels of human glioblastoma multiforme. *Acta Neuropathol.* **100**, 323–331 (2000).
- 8 15. Wolburg, H. *et al.* Localization of claudin-3 in tight junctions of the blood-brain barrier is
9 selectively lost during experimental autoimmune encephalomyelitis and human glioblastoma
10 multiforme. *Acta Neuropathol.* **105**, 586–592 (2003).
- 11 16. Pointer, K. B. *et al.* Association of collagen architecture with glioblastoma patient survival. *J.*
12 *Neurosurg.* **126**, 1812 (2017).
- 13 17. Reardon, D. A. *et al.* Glioblastoma eradication following immune checkpoint blockade in an
14 orthotopic, immunocompetent model. *Cancer Immunol. Res.* **4**, 124–135 (2016).
- 15 18. Park, J. *et al.* Effect of combined anti-PD-1 and temozolomide therapy in glioblastoma.
16 *Oncoimmunology* **8**, (2018).
- 17 19. Reardon, D. A. *et al.* Effect of Nivolumab vs Bevacizumab in Patients With Recurrent
18 Glioblastoma: The CheckMate 143 Phase 3 Randomized Clinical Trial. *JAMA Oncol.* **6**, 1003–1010
19 (2020).
- 20 20. Louis, D. N. *et al.* The 2021 WHO classification of tumors of the central nervous system: A
21 summary. *Neuro. Oncol.* **23**, (2021).
- 22 21. Basch, E. & Schrag, D. The Evolving Uses of ‘Real-World’ Data. *JAMA* vol. 321 (2019).
- 23 22. Urup, T. *et al.* Development and validation of a prognostic model for recurrent glioblastoma
24 patients treated with bevacizumab and irinotecan. *Acta Oncol. (Madr).* **55**, (2016).
- 25 23. Giunti, D. *et al.* Phenotypic and functional analysis of T cells homing into the CSF of subjects with
26 inflammatory diseases of the CNS. *J. Leukoc. Biol.* **73**, 584–590 (2003).
- 27 24. Teleshova, N. *et al.* Multiple sclerosis and optic neuritis: CCR5 and CXCR3 expressing T cells are

- 1 augmented in blood and cerebrospinal fluid. *J. Neurol.* **249**, 723–729 (2002).
- 2 25. Osa, A. *et al.* Clinical implications of monitoring nivolumab immunokinetics in non–small cell lung
3 cancer patients. *JCI Insight* **3**, (2018).
- 4 26. Duhén, T. *et al.* Co-expression of CD39 and CD103 identifies tumor-reactive CD8 T cells in human
5 solid tumors. *Nat. Commun.* **9**, 1–13 (2018).
- 6 27. Wolfl, M. *et al.* Activation-induced expression of CD137 permits detection, isolation, and
7 expansion of the full repertoire of CD8+ T cells responding to antigen without requiring
8 knowledge of epitope specificities. *Blood* **110**, 201–210 (2007).
- 9 28. Chow, A. *et al.* The ectonucleotidase CD39 identifies tumor-reactive CD8+ T cells predictive of
10 immune checkpoint blockade efficacy in human lung cancer. *Immunity* **56**, 93–106 (2023).
- 11 29. Kverneland, A. H. *et al.* Adoptive cell therapy with tumor-infiltrating lymphocytes supported by
12 checkpoint inhibition across multiple solid cancer types. *J. Immunother. Cancer* **9**, 3499 (2021).
- 13 30. Krishna, S. *et al.* Stem-like CD8 T cells mediate response of adoptive cell immunotherapy against
14 human cancer. *Science (80-.)*. **370**, 1328 (2020).
- 15 31. Kortekaas, K. E. *et al.* CD39 identifies the CD4+ tumor-specific T-cell population in human cancer.
16 *Cancer Immunol. Res.* **8**, 1311–1321 (2020).
- 17 32. Voskoboinik, I., Smyth, M. J. & Trapani, J. A. Perforin-mediated target-cell death and immune
18 homeostasis. *Nature Reviews Immunology* vol. 6 (2006).
- 19 33. Zheng, C. *et al.* Landscape of Infiltrating T Cells in Liver Cancer Revealed by Single-Cell
20 Sequencing. *Cell* **169**, (2017).
- 21 34. Kim, K. H. *et al.* PD-1 blockade-unresponsive human tumor-infiltrating CD8+ T cells are marked by
22 loss of CD28 expression and rescued by IL-15. *Cell. Mol. Immunol.* **18**, (2021).
- 23 35. Kamphorst, A. O. *et al.* Rescue of exhausted CD8 T cells by PD-1 targeted therapies is CD28-
24 dependent. *Science (80-.)*. **355**, 1423 (2017).
- 25 36. Hui, E. *et al.* T cell costimulatory receptor CD28 is a primary target for PD-1-mediated inhibition.
26 *Science (80-.)*. **355**, 1428–1433 (2017).
- 27 37. Baghbani, E. *et al.* Regulation of immune responses through CD39 and CD73 in cancer: Novel

- 1 checkpoints. *Life Sci.* **282**, 119826 (2021).
- 2 38. Peres, R. S. *et al.* TGF- β signalling defect is linked to low CD39 expression on regulatory T cells
3 and methotrexate resistance in rheumatoid arthritis. *J. Autoimmun.* **90**, (2018).
- 4 39. Arab, S. & Hadjati, J. Adenosine blockage in tumor microenvironment and improvement of cancer
5 immunotherapy. *Immune Netw.* **19**, (2019).
- 6 40. Cendrowski, J., Mamińska, A. & Miaczynska, M. Endocytic regulation of cytokine receptor
7 signaling. *Cytokine Growth Factor Rev.* **32**, 63–73 (2016).
- 8 41. Saad, E. Ben, Oroya, A. & Rudd, C. E. Abstract 6528: Anti-PD-1 induces the endocytosis of the co-
9 receptor from the surface of T-cells: Nivolumab is more effective than Pembrolizumab. *Cancer*
10 *Res.* **80**, (2020).
- 11 42. Jenkins, R. W., Barbie, D. A. & Flaherty, K. T. Mechanisms of resistance to immune checkpoint
12 inhibitors. *Br. J. Cancer* **118**, (2018).
- 13 43. Hung, A. L. *et al.* TIGIT and PD-1 dual checkpoint blockade enhances antitumor immunity and
14 survival in GBM. *Oncoimmunology* **7**, (2018).
- 15 44. Raphael, I. *et al.* TIGIT and PD-1 Immune Checkpoint Pathways Are Associated With Patient
16 Outcome and Anti-Tumor Immunity in Glioblastoma. *Front. Immunol.* **12**, (2021).
- 17 45. Dhatchinamoorthy, K., Colbert, J. D. & Rock, K. L. Cancer Immune Evasion Through Loss of MHC
18 Class I Antigen Presentation. *Front. Immunol.* **12**, (2021).
- 19 46. Lee, M. Y., Jeon, J. W., Sievers, C. & Allen, C. T. Antigen processing and presentation in cancer
20 immunotherapy. *J. Immunother. cancer* **8**, (2020).
- 21 47. Scheer, M. *et al.* Neurofibromatosis type 1 gene alterations define specific features of a subset of
22 glioblastomas. *Int. J. Mol. Sci.* **23**, (2022).
- 23 48. Lobbous, M. *et al.* An update on neurofibromatosis type 1-associated gliomas. *Cancers (Basel).*
24 **12**, (2020).
- 25 49. Zhang, J. *et al.* The combination of neoantigen quality and T lymphocyte infiltrates identifies
26 glioblastomas with the longest survival. *Commun. Biol.* **2**, (2019).
- 27 50. Hilf, N. *et al.* Actively personalized vaccination trial for newly diagnosed glioblastoma. *Nature*

1 **565**, (2019).

2 51. Keskin, D. B. *et al.* Neoantigen vaccine generates intratumoral T cell responses in phase Ib
3 glioblastoma trial. *Nature* **565**, (2019).

4 52. Leko, V. *et al.* Identification of neoantigen-reactive T lymphocytes in the peripheral blood of a
5 patient with glioblastoma. *J. Immunother. Cancer* **9**, (2021).

6 53. Holm, J. S. *et al.* Neoantigen-specific CD8 T cell responses in the peripheral blood following PD-L1
7 blockade might predict therapy outcome in metastatic urothelial carcinoma. *Nat. Commun.* **13**,
8 (2022).

9 54. Thall, P. F., Simon, R., Ellenberg, S. S. & Shrager, R. Optimal two-stage designs for clinical trials
10 with binary response. *Stat. Med.* **7**, (1988).

11 55. Donia, M. *et al.* Characterization and comparison of ‘standard’ and ‘young’ tumour-infiltrating
12 lymphocytes for adoptive cell therapy at a Danish translational research institution. *Scand. J.*
13 *Immunol.* **75**, 157–67 (2012).

14 56. Andersen, R. *et al.* T cells isolated from patients with checkpoint inhibitor-resistant melanoma
15 are functional and can mediate tumor regression. *Ann. Oncol.* **29**, 1575–1581 (2018).

16 57. Draghi, A. *et al.* Rapid Identification of the Tumor-Specific Reactive TIL Repertoire via Combined
17 Detection of CD137, TNF, and IFN γ , Following Recognition of Autologous Tumor-Antigens. *Front.*
18 *Immunol.* **12**, 4236 (2021).

19 58. Krueger, F. Trim Galore. <https://github.com/FelixKrueger/TrimGalore> (2019).

20 59. Martin, M. Cutadapt removes adapter sequences from high-throughput sequencing reads.
21 *EMBnet.journal* **17**, (2011).

22 60. Andrews, S. FastQC. <https://www.bioinformatics.babraham.ac.uk/projects/fastqc> (2019).

23 61. Lab, P. Kallisto. <https://pachterlab.github.io/kallisto/> (2019).

24 62. Consortium, G. R. Genome Reference Consortium Human Build 38 patch release 14
25 (GRCh38.p14). https://www.ncbi.nlm.nih.gov/assembly/GCF_000001405.40 (2022).

26 63. Mundt, F. *et al.* In depth profiling of the cancer proteome from the flowthrough of standard RNA-
27 preparation kits for precision oncology. *bioRxiv* 2023.05.12.540582 (2023)

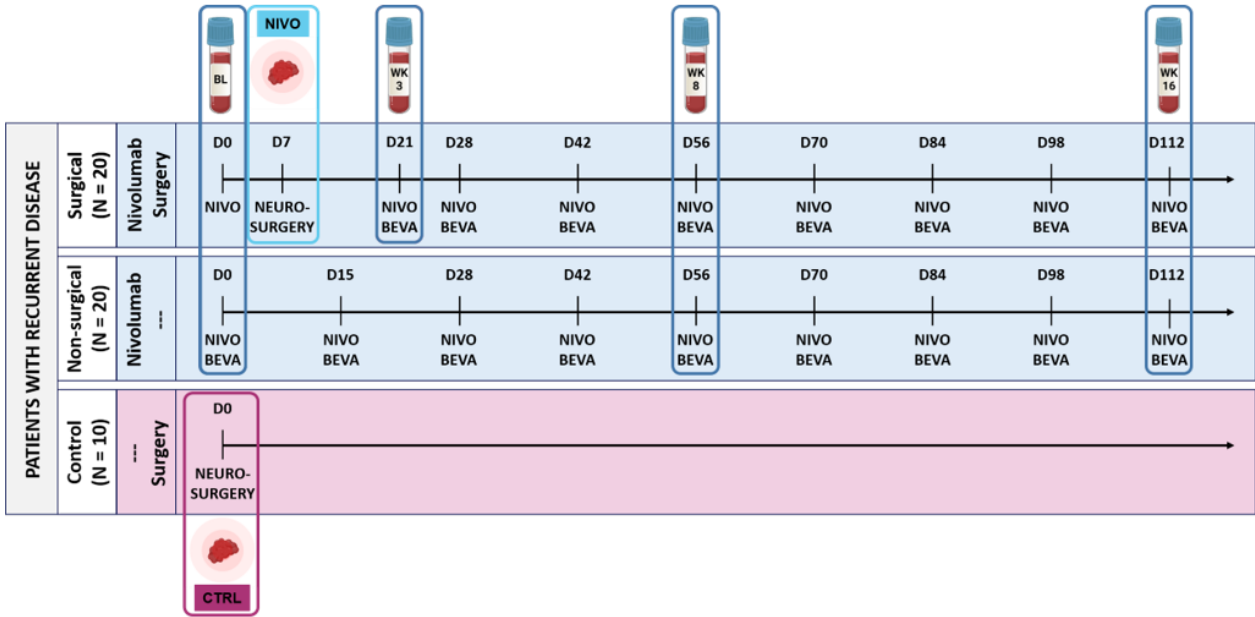
doi:10.1101/2023.05.12.540582.

64. Geyer, P. E. *et al.* Plasma Proteome Profiling to Assess Human Health and Disease. *Cell Syst.* **2**, (2016).
65. Meier, F. *et al.* diaPASEF: parallel accumulation–serial fragmentation combined with data-independent acquisition. *Nat. Methods* **17**, (2020).
66. Love, M. I., Huber, W. & Anders, S. Moderated estimation of fold change and dispersion for RNA-seq data with DESeq2. *Genome Biol.* **15**, (2014).
67. Wu, T. *et al.* clusterProfiler 4.0: A universal enrichment tool for interpreting omics data. *Innov.* **2**, (2021).
68. Gu, Z., Eils, R. & Schlesner, M. Complex heatmaps reveal patterns and correlations in multidimensional genomic data. *Bioinformatics* **32**, (2016).
69. Yu, G. Visualization of functional enrichment result. R package version 1.10.2. *Mol. Ther. Nucleic Acids* (2021).
70. McKenna, A. *et al.* The Genome Analysis Toolkit: a MapReduce framework for analyzing next-generation DNA sequencing data. *Genome Res.* **20**, (2010).
71. Li, H. Aligning sequence reads, clone sequences and assembly contigs with BWA-MEM. *arXiv Prepr. arXiv* (2013).
72. Cibulskis, K. *et al.* Sensitive detection of somatic point mutations in impure and heterogeneous cancer samples. *Nat. Biotechnol.* **31**, (2013).
73. Bjerregaard, A. M., Nielsen, M., Hadrup, S. R., Szallasi, Z. & Eklund, A. C. MuPeXI: prediction of neo-epitopes from tumor sequencing data. *Cancer Immunol. Immunother.* **66**, 1123–1130 (2017).
74. Reynisson, B., Alvarez, B., Paul, S., Peters, B. & Nielsen, M. NetMHCpan-4.1 and NetMHCIIpan-4.0: Improved predictions of MHC antigen presentation by concurrent motif deconvolution and integration of MS MHC eluted ligand data. *Nucleic Acids Res.* **48**, (2021).
75. Weese, D., Holtgrewe, M. & Reinert, K. RazerS 3: Faster, fully sensitive read mapping. *Bioinformatics* **28**, (2012).
76. Szolek, A. *et al.* OptiType: precision HLA typing from next-generation sequencing data.

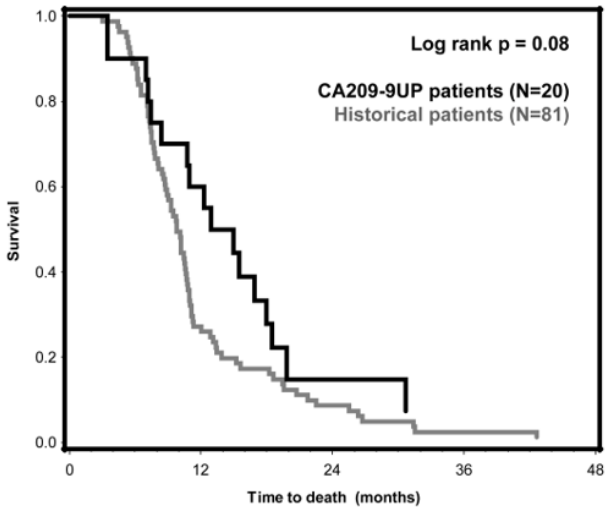
- 1 *Bioinformatics* **30**, 3310 (2014).
- 2 77. Bentzen, A. K. *et al.* Large-scale detection of antigen-specific T cells using peptide-MHC-I
- 3 multimers labeled with DNA barcodes. *Nat. Biotechnol.* **34**, 1037–1045 (2016).
- 4

Main Figures

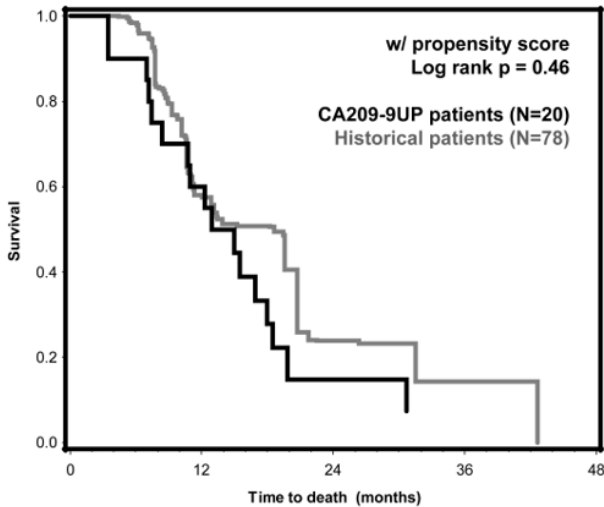
a



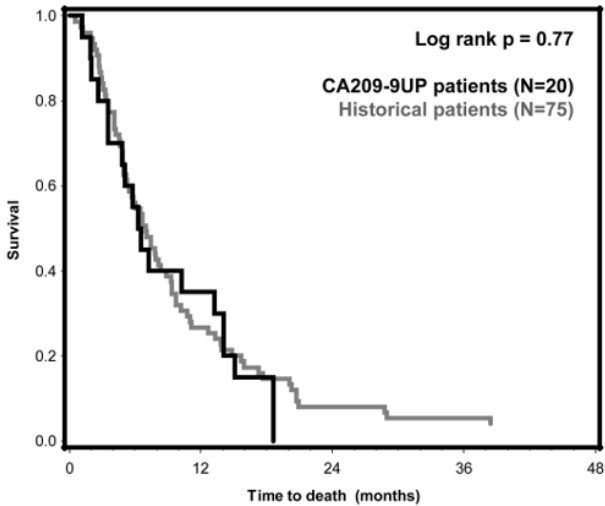
b



c



d



e

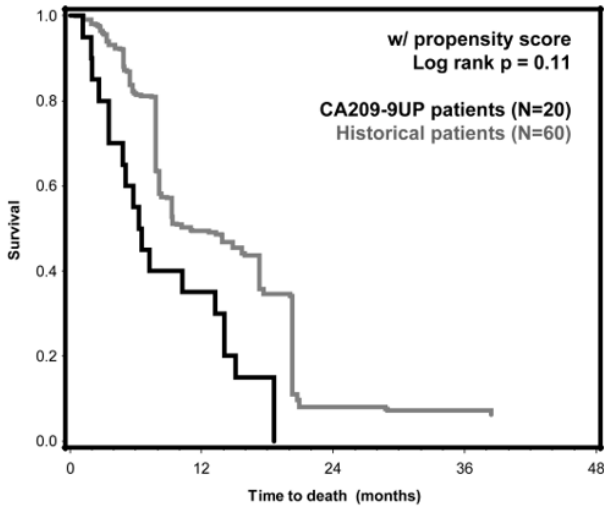


Figure 1 Clinical setup and survival. a) Timeline showing administration of treatment with Nivolumab (NIVO) and Bevacizumab (BEVA), including time points of sampling blood and tumor. Treated patients (blue) included a surgical group and non-surgical group, and all patients received Nivolumab and Bevacizumab every two weeks. Patients in the surgical group also received Nivolumab seven days prior surgery. Control patients (purple) with recurrent glioblastoma undergoing neurosurgical resection were additionally included. These patients did not receive Nivolumab before resection. Additionally, blood samples were collected from treated patients at Day 0 as baseline (BL), after 8 weeks (WK 8) and 16 weeks (WK 16). An additional blood sample was collected from patients in surgical group 3 weeks (WK 3) after Nivolumab administration (2 weeks after surgery). **b-e)** Overall survival by Kaplan-Meier curves comparing patients in our CA209-9UP clinical trial (N=40, black line) with a historical patient group (N=156, grey line) from our one-site database, who were treated with bevacizumab and irinotecan from 2006-2014, but not Nivolumab. All patients were subdivided in **b-c)** a surgical group and **d-e)** a non-surgical group. Comparison between the historical patient group and the patient in trial was done **b&d)** without using propensity scores and **c&e)** weighted using propensity scores based on age, gender, corticosteroid use, multifocal disease, MGMT status and extent of resection.

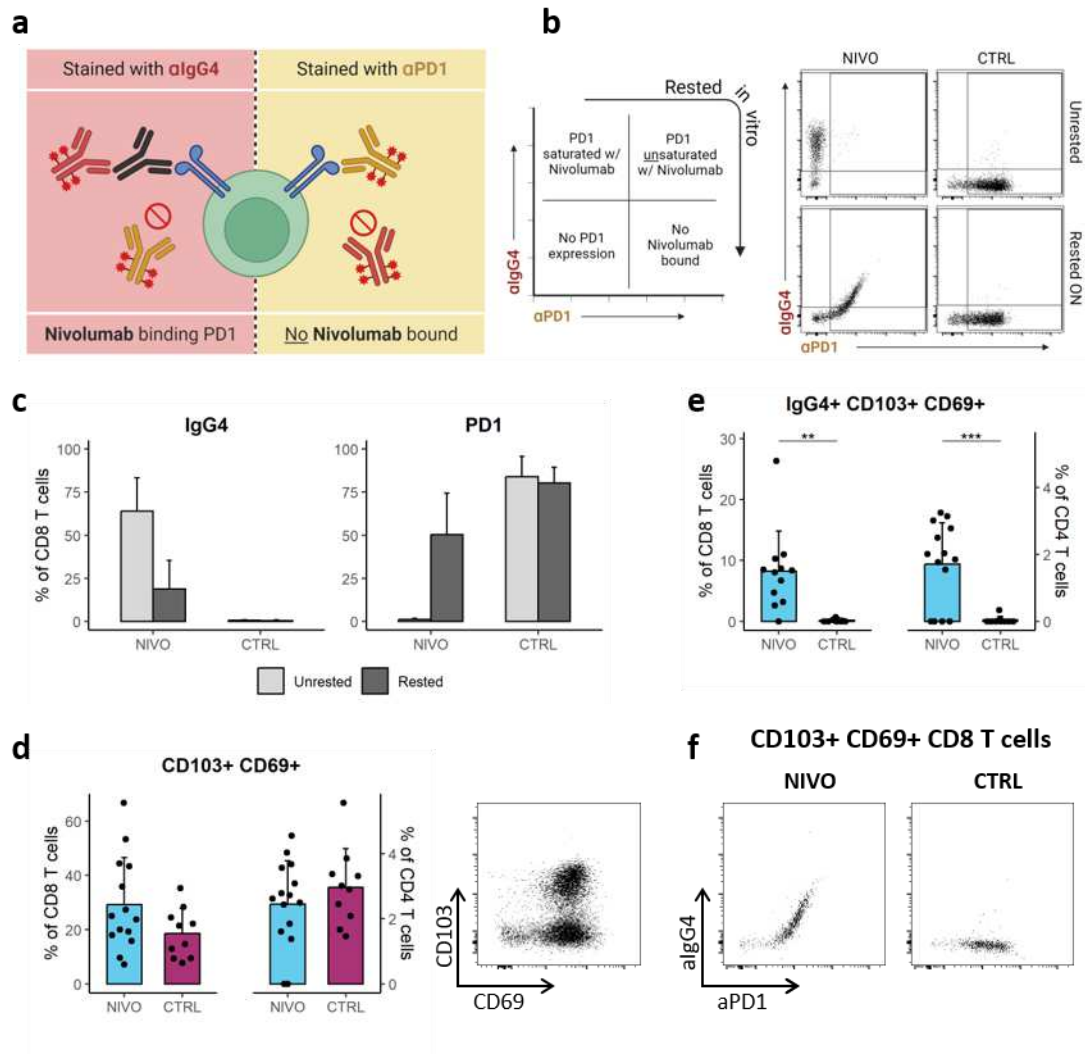


Figure 2 Intratumoral detection of Nivolumab and tissue resident T-cells. **a)** Illustrative explanation for PD1 and Nivolumab antibody (Ab)-detection; Nivolumab bound to PD1 was detected with a fluorochrome-conjugated anti-IgG4 Ab (red) binding to the Fc region of Nivolumab (black Ab), while free PD1 molecules were detected with fluorochrome-labelled anti-PD1 Ab (yellow). **b)** Explanation of dot plot showing Nivolumab binding and saturation (left), representative flow cytometry dot plots of unrested and rested tumor digest stained with aPD1 and algG4, showing a complete Nivolumab saturation of intratumoral T-cells in unrested tumor digest from Nivolumab-treated (NIVO) patient, which is partly lost after resting. Intratumoral T-cells from control (CTRL) patients do not bind algG4 (right). **c)** Frequency of CD8+ T-cells stained with algG4 (Nivolumab bound) and aPD1 (free PD1 molecules) in unrested (light grey) and rested (dark grey) tumor digest. **d)** Frequency of CD8+ and CD4+ T-cells co-expressing the markers of tissue residency, CD69 and CD103, in Tumor digest from NIVO patients (light blue) and CTRL patients (purple) (left). Representative plot of intratumoral CD8+ T-cells expressing CD69 and CD103 (right). **e)** Frequency of CD8+ and CD4+ T-cells binding Nivolumab (algG4) that are tissue resident T-cells. **f)** Representative plots from NIVO and CTRL patients showing tissue resident CD8+ T-cells from rested tumor digest binding aPD1 and algG4. Means were compared between NIVO and CTRL using unpaired t-test. * = $p < 0.05$, ** = $p < 0.01$, *** = $p < 0.001$, **** = $p < 0.0001$.

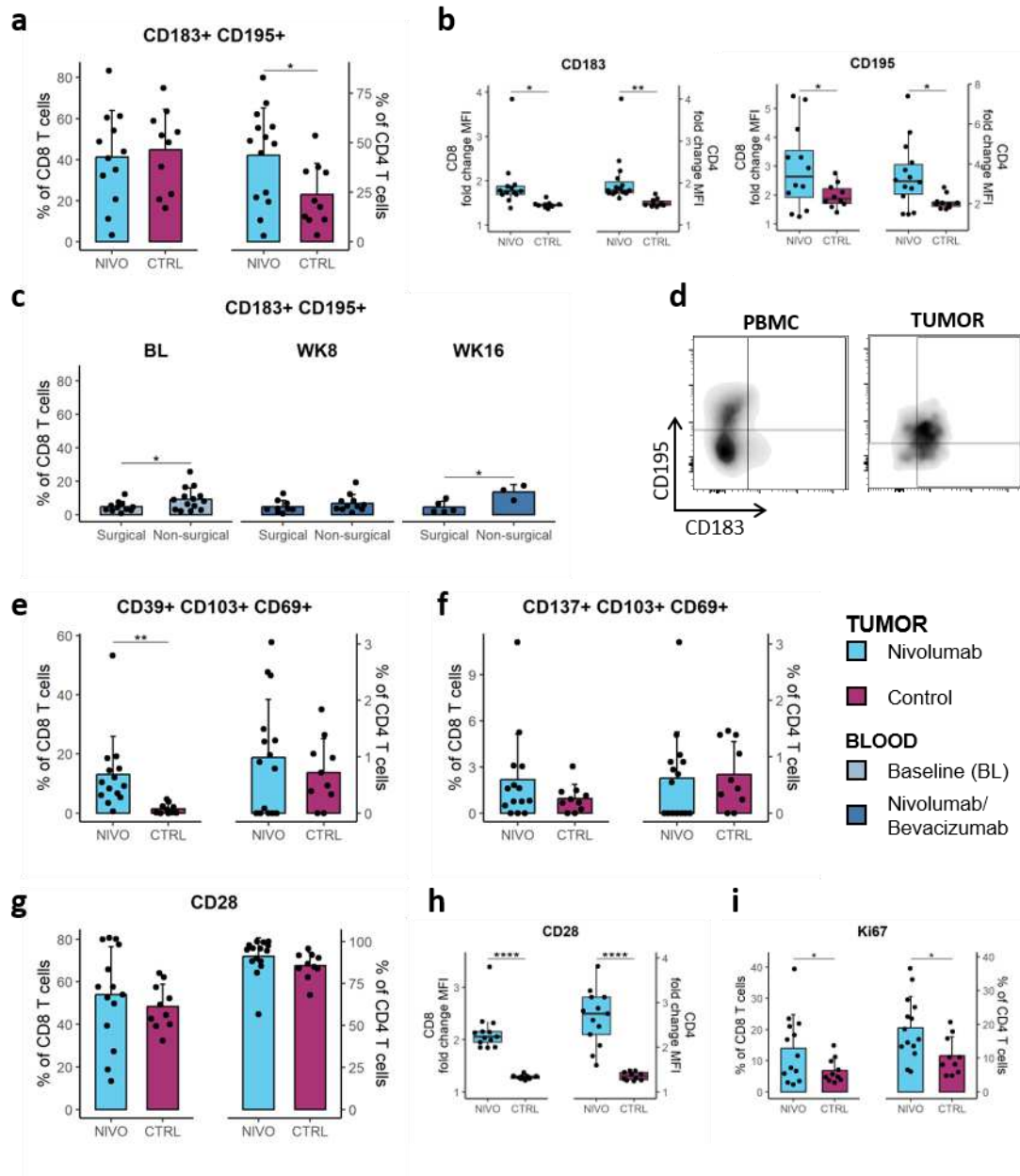


Figure 3 CNS-homing, activation and proliferation in tumor tissue and blood. **a)** Frequency of CD8+ and CD4+ T-cells co-expressing the chemokine receptors, CD183 (CXCR3) and CD195 (CCR5) in tumor tissue of Nivolumab-treated (NIVO) and control (CTRL) patients, for indication of CNS homing. **b)** Fold change in median fluorescent intensity (MFI) between the positive and negative population in T-cells stained for CD183 and CD195. MFI fold change indicate the change in expression level of the two markers in NIVO and CTRL patients. **c)** Frequency of CD8+ T-cells co-expressing CD183 and CD195 in blood samples from Baseline (BL), week (WK) 8 and WK16. Frequencies are compared between the surgical group and the tumor bearing group (non-surgical group). **d)** Representative flow cytometry plot of CD195 and CD183 staining in blood (PBMCs) and tumor. **e)** Frequency of tissue resident T-cells expressing CD39 among intratumoral CD8+ and CD4+ T-cells. **f)** Frequency of tissue resident T-cells expressing CD137 among intratumoral CD8+ and CD4+ T-cells. **g)** Frequency of T-cells expressing CD28 among intratumoral CD8+ and CD4+ T-cells. **h)** MFI fold change of CD28 staining of intratumoral CD8+ and CD4+ T-cells. **i)** Frequency of T-cells expressing Ki67 among intratumoral CD8+ and CD4+ T-cells. Means were compared between NIVO and CTRL (Tumor), and between surgical group and non-surgical group (blood) using unpaired t-test. * = $p < 0.05$, ** = $p < 0.01$, *** = $p < 0.001$, **** = $p < 0.0001$.

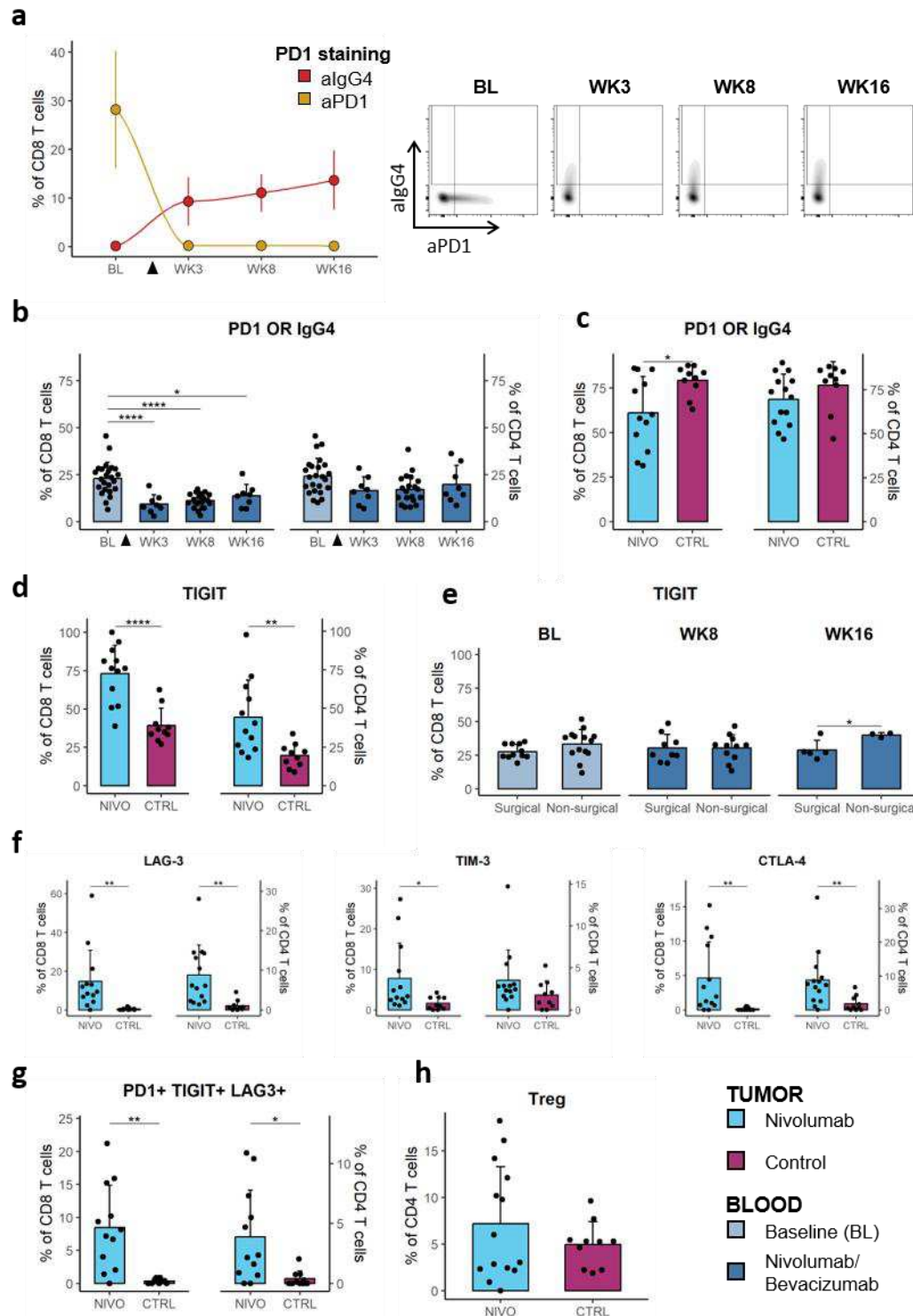


Figure 4 Nivolumab induced differentiation of T-cells. **a)** The kinetics of Nivolumab binding. CD8+ T-cells derived from blood collected before (BL) and after (WK3, WK8, WK16) Nivolumab administration stained with aPD1 (yellow) and algG4 (red). **b)** Frequency of a collected PD1+ population (based on aPD1 and algG4 staining) within PBMC derived T-cells collected at different time points of the treatment. **c)** Frequency of the collected PD1+ population within intratumoral T-cells from Nivolumab-treated (NIVO) and control (CTRL) patients. **d)** Frequency of intratumoral T-cells from NIVO and CTRL patients expressing TIGIT. **e)** Frequency of CD8+ T-cells expressing TIGIT from blood samples at baseline (BL), week (WK) 3, WK8 and WK16. Comparing the surgical group to the tumor bearing group (non-surgical group). **f)** Frequency of intratumoral T-cells from NIVO and CTRL patients expressing LAG-3, TIM-3 and CTLA-4. **g)** Frequency of intratumoral T-cells co-expressing PD1+, TIGIT+ and LAG-3 from NIVO and CTRL patients. **h)** Frequency Treg cells among intratumoral CD4+ T-cells from NIVO and CTRL patients. Means were compared between NIVO and CTRL (Tumor), and between group A and group B, and the four time points (blood) using unpaired t-test. * = $p < 0.05$, ** = $p < 0.01$, *** = $p < 0.001$, **** = $p < 0.0001$.

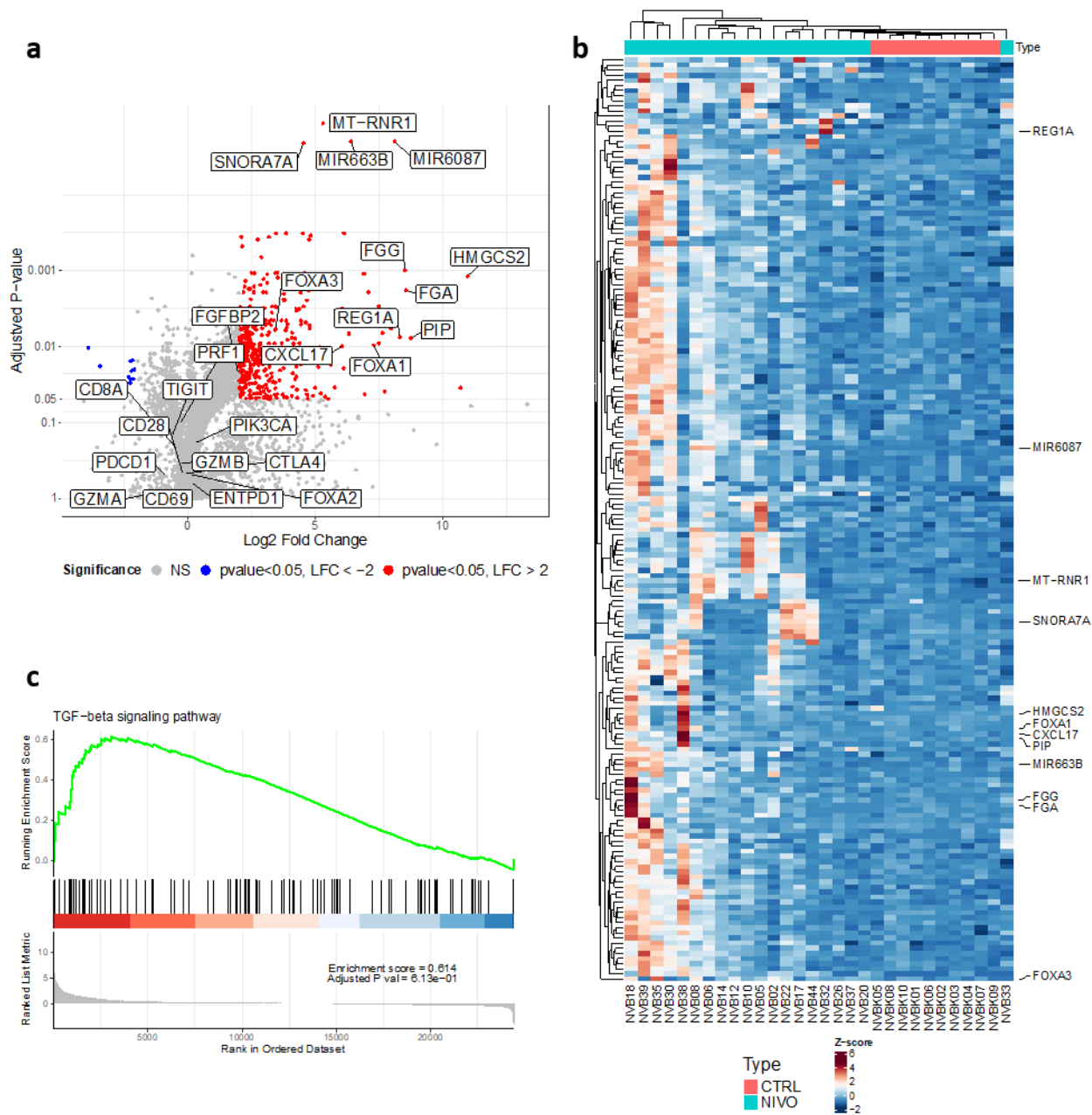


Figure 5 Transcriptomic comparison of Nivolumab treated patients versus control. **a)** Volcano plot showing 1,716 differential overexpressed genes, in red those with an adjusted p-value < 0.05 and log2 fold change > 2. Additionally, 260 under-expressed genes was found, in blue those with adjusted p-value < 0.05 and log2 fold change < -2. The highlighted genes consist of the most up/down regulated genes and few immune-related genes of interest. Additionally, the genes asses by in flow cytometry are highlighted. **b)** The most significantly differential expressed genes from the volcano figure with adjusted p-value < 0.01 and log2 fold change > 2 or < -2 were illustrated with a heatmap with unsupervised clustering. Highlighted genes are significantly over and under-expressed genes highlighted in a). **c)** A gene set enrichment analysis showed that the TGF- β pathway were differential over-expressed in the Nivolumab treated patients shown in an enrichment figure.

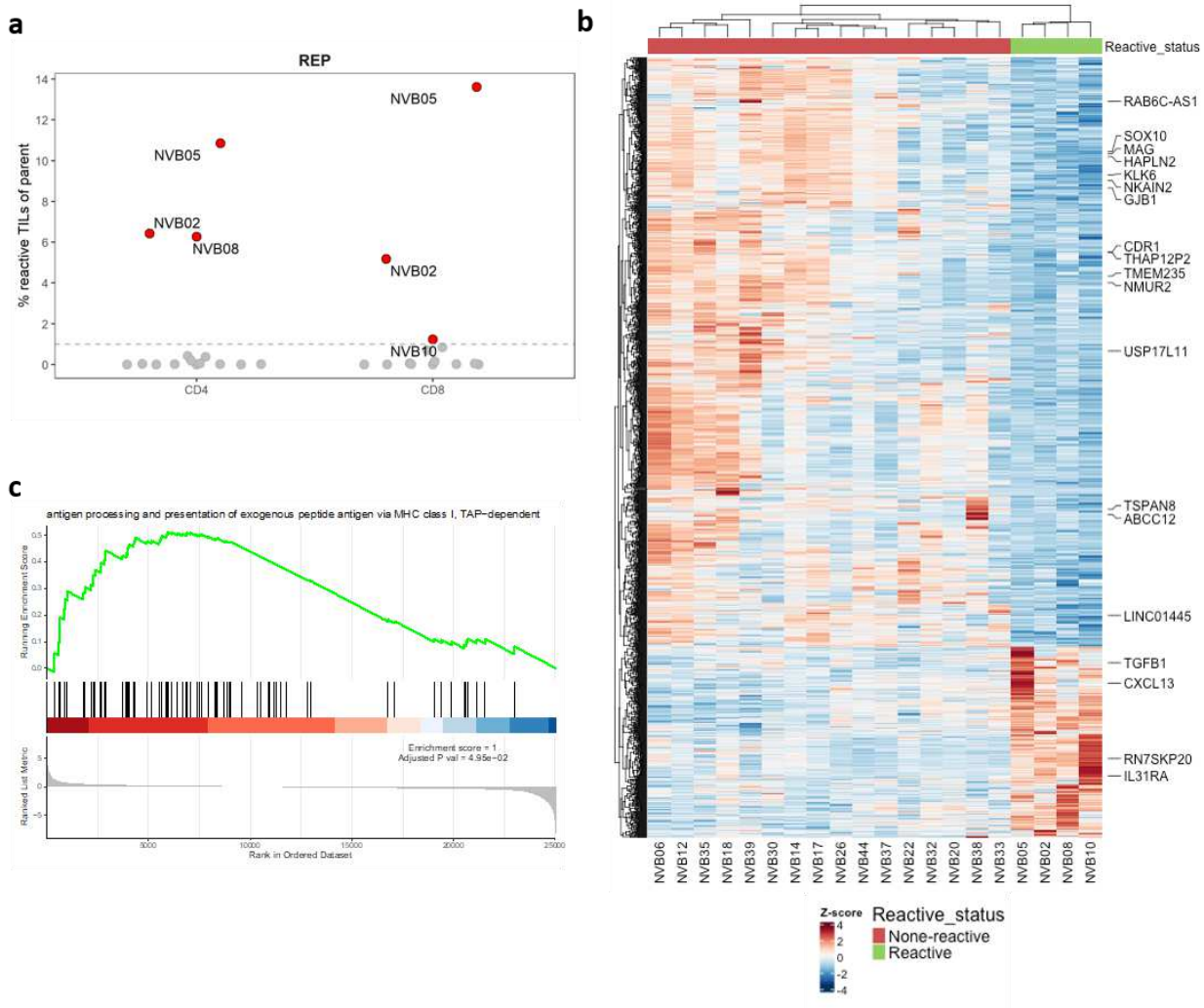


Figure 6 Comparison of patients with reactive T-cells versus non-reactive T-cells. a) Reactivity towards autologous tumor digest detected in REP TILs. TILs where co-cultured with autologous tumor digest for 8 hours and hereafter intracellularly stained for TFN- α , IFN- γ , CD137 and surface stained for CD107a. TILs expressing at least two of the markers, where defined as reactive. Background reactivity (TILs alone) are subtracted and hereafter patients with more than 1% reactive TILs are defined as reactive. Patients with tumor reactive TILs are highlighted in red. Patients without tumor reactive TILs are marked in grey. **b)** 372 differential over-expressed and 1,150 differential under-expressed genes were found in patients with reactive T-cells by differential expression analysis with adjusted p-value < 0.05. These differentially expressed genes were illustrated by heatmap showing that patients with reactive and non-reactive T-cells were defining the two first unsupervised clusters. The highlighted genes consist of the most up/down regulated genes and include some immune-related genes of interest. **c)** A gene set enrichment analysis was made from the DEA and antigen presentation on MHC-I was found as enriched pathway for patients with reactive T-cells.

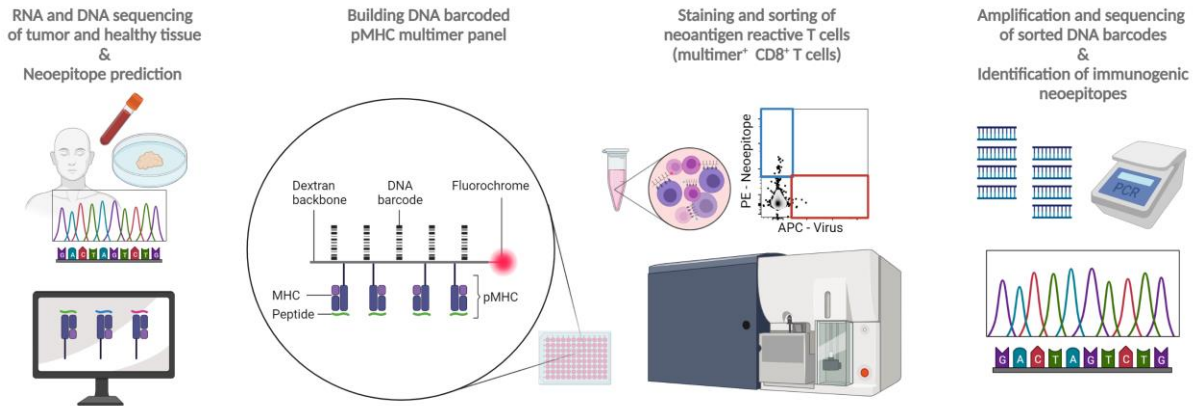
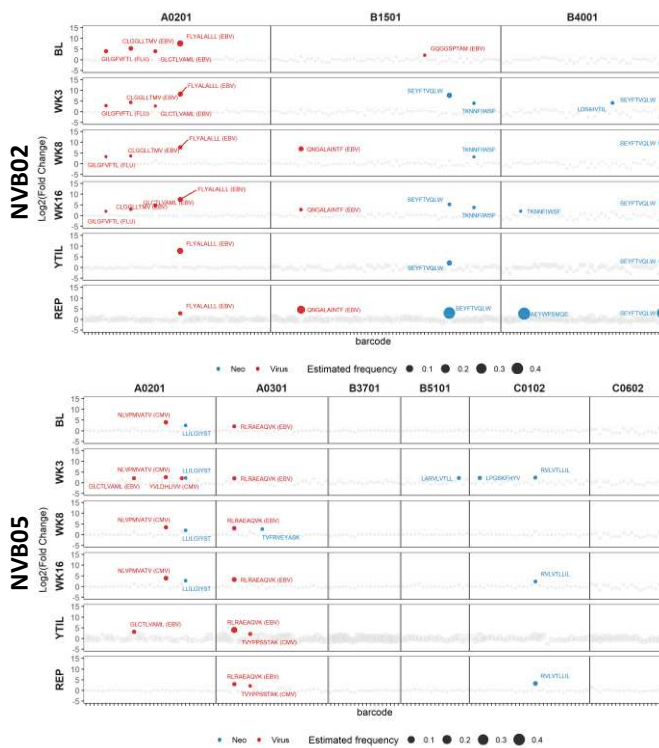
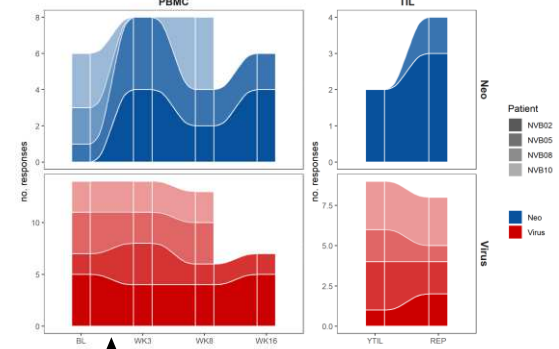
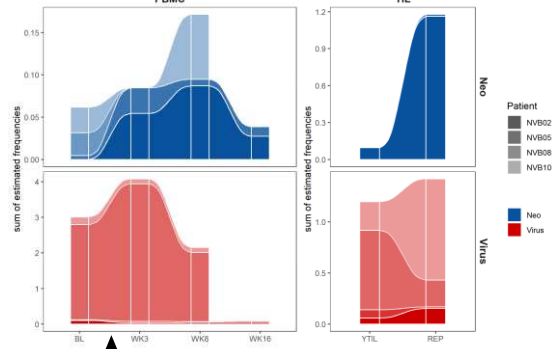
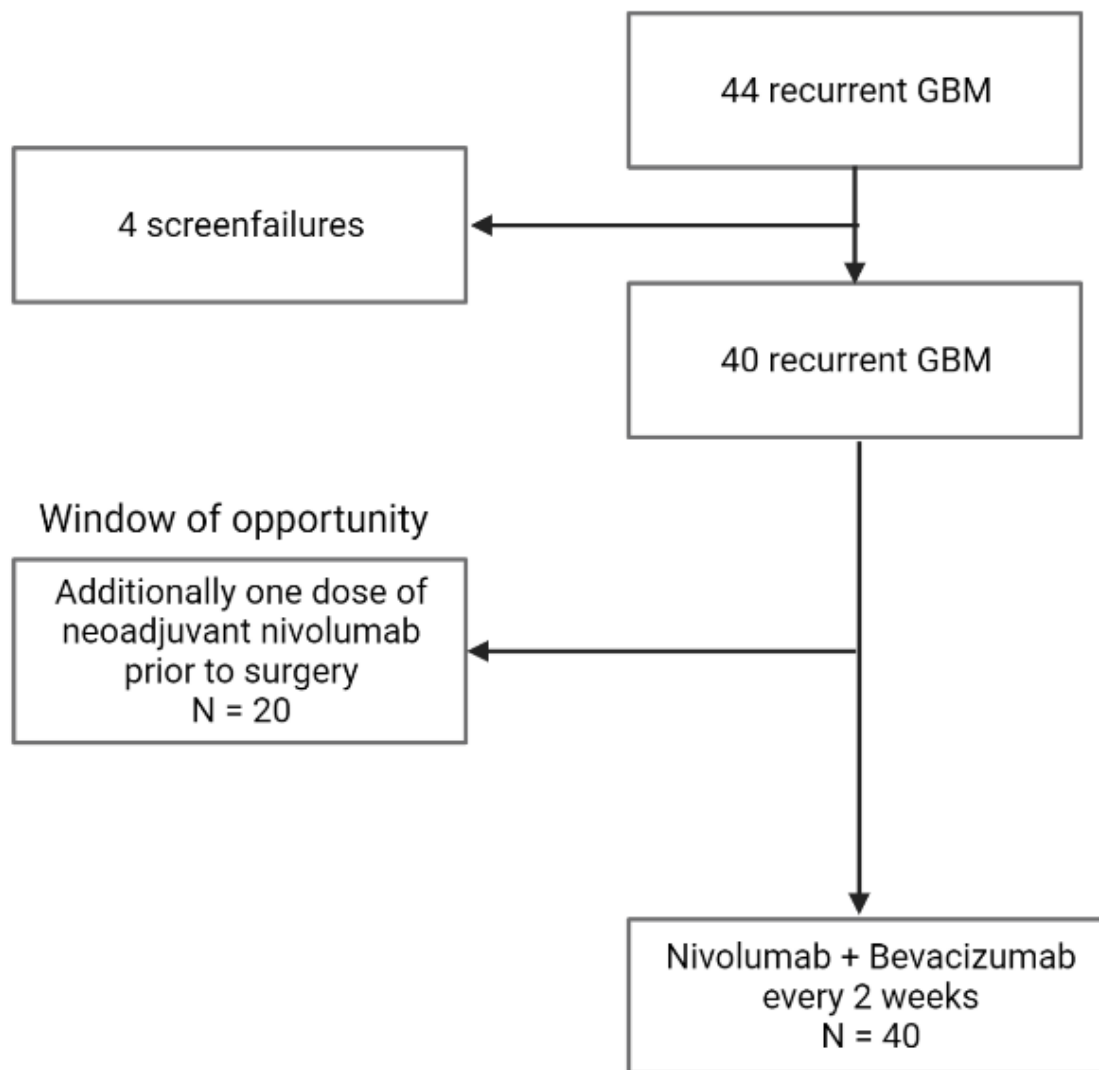
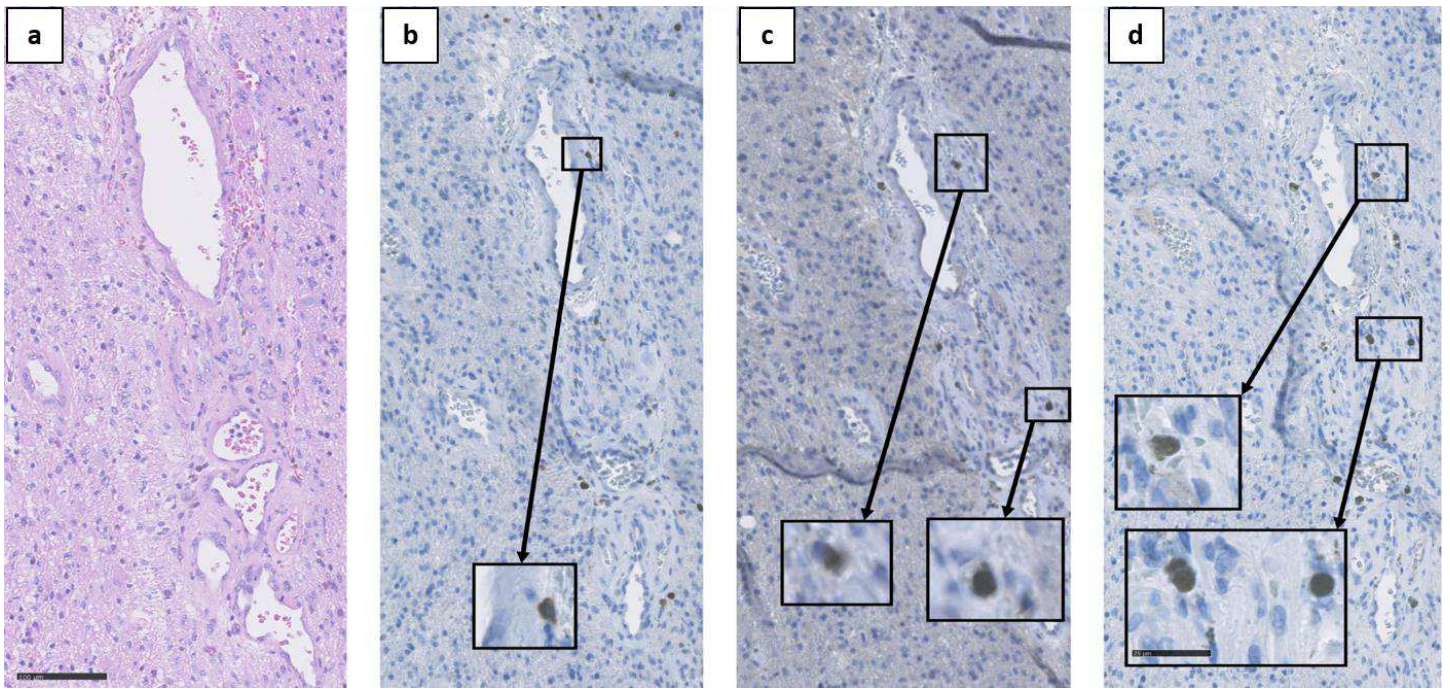
a**b****d****e**

Figure 7 Detection of neo-antigen reactive CD8⁺ T-cells (NARTs). **a)** Illustrative explanation of NART detection. Neoantigens were predicted based on whole exome sequencing (WES) and RNA sequencing of tumor and WES of healthy tissue (blood). A patient specific panel of DNA-barcoded pMHC multimers, was assembled with the predicted neopeptides and virus peptides. Patient material (TILs and PBMCs) were stained with a pool of the multimer panel, and multimer⁺ CD8⁺ T-cells were sorted based on their fluorochrome label; PE (blue) for neopeptides and APC (red) for virus peptides. The DNA-barcodes bound to the sorted T-cells were hereafter amplified by PCR and sequenced. Enriched and hereby immunogenic neopeptides- and virus peptides-MHC complexes were identified based on the corresponding DNA-barcode. **b)** Screening output for patient NVB02 and NVB05. Significantly enriched ($p < 0.001$, Log₂ fold change > 2) barcoded pMHC multimers are colored and labelled with the immunogenic peptide sequence. Virus antigens are marked in red and neoantigens are marked in blue. The dot size represents an estimated frequency of CD8⁺ T-cells for each NART. Grey dots are all pMHC multimers that were not significantly enriched after sample staining. Specificities are shown for each blood sample timepoint; Baseline (BL), week (WK) 3, WK8, WK16, and for young TILs (YTIL) and rapidly expanded (REP) TILs. The screened pMHC are additionally divided based on HLA type. **c)** Number of responses towards different neoantigens (blue) and virus antigens (red). Individual patients are marked in different shades of the respective color. The plot is further divided in PBMC and TILs. There was no significant difference between blood-sample time points or between YTILs and REP TILs. **d)** Sum of estimated frequency of NARTs recognizing different neoantigens (blue) and virus antigens (red). There was also no significant difference between blood sample time points or between YTILs and REP TILs.

Supplementary Figures

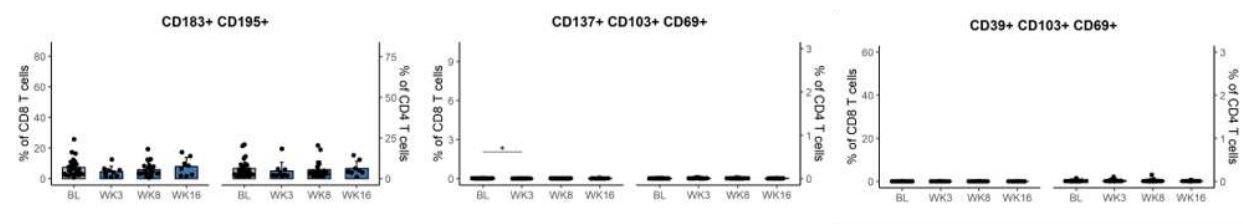


Supplementary Figure 1 Clinical trial setup. 40 patients included with recurrent glioblastoma which had received Stupp's regimen at primary diagnosis. If they underwent neurosurgical resection, we used the window of opportunity and gave them one dose of neoadjuvant nivolumab. Tumor samples from the neurosurgical resection could later be used for pharmacokinetics and pharmacodynamics analyses.

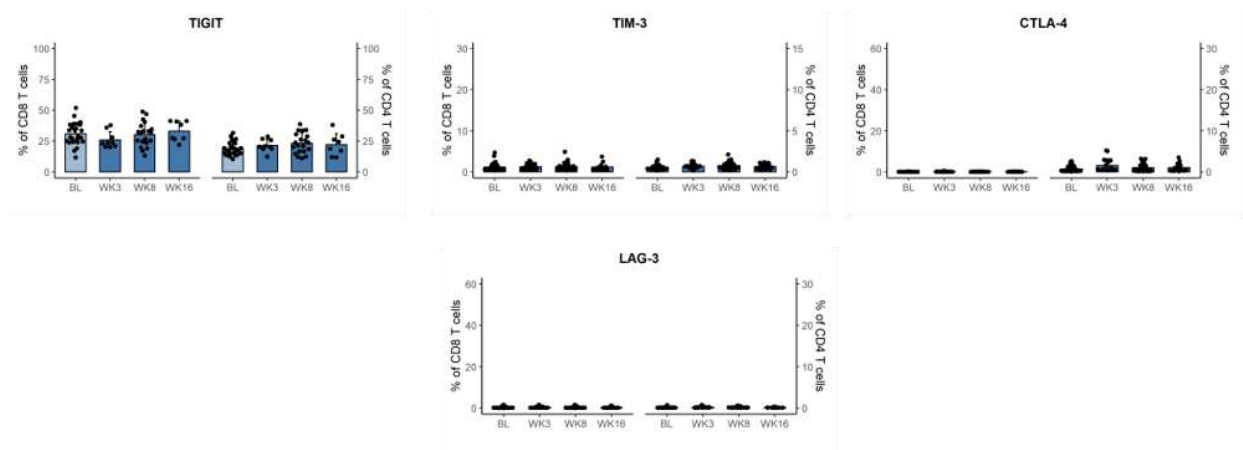


Supplementary Figure 2 Staining for Nivolumab in histological sections of tumor from Nivolumab treated patients. Consecutive histological sections from tumor tissue from Nivolumab treated patients with recurrent GBM were immunohistochemically stained with CD3, PD-1 and IgG4 to demonstrate localization of Nivolumab - a human monoclonal antibody of IgG4 isotype - in the tumor tissue (Patient NVB20). **a)** Hematoxylin and eosin staining. **b)** Staining for CD3 demonstrating presence of T cells in the tumor area. **c)** PD-1+ cells with T-cell morphology in the tumor area. **d)** IgG4+ cells with T-cell morphology in the tumor area. Images were acquired at 20X magnification with scale bars = 100 μm and at 80X magnification with scale bar = 25 μm (insert).

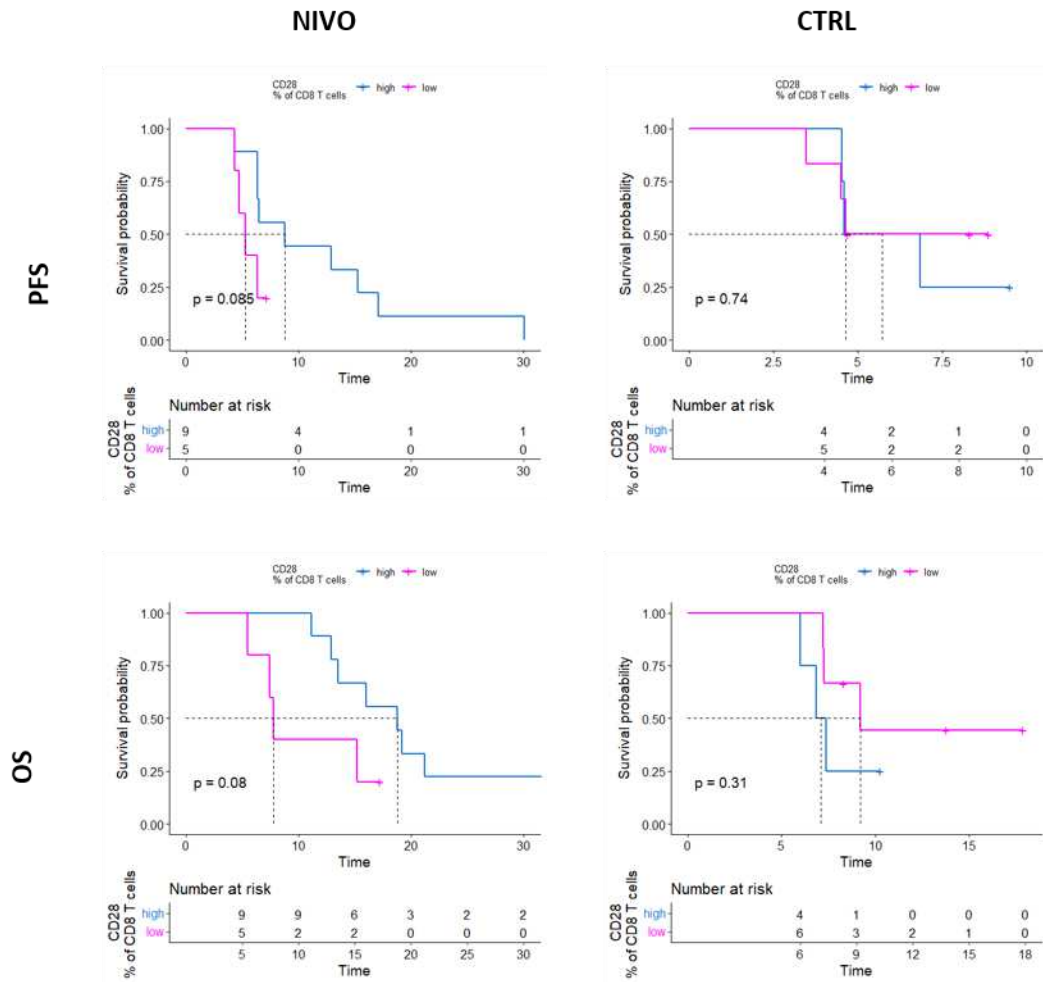
CNS homing and activated T cells



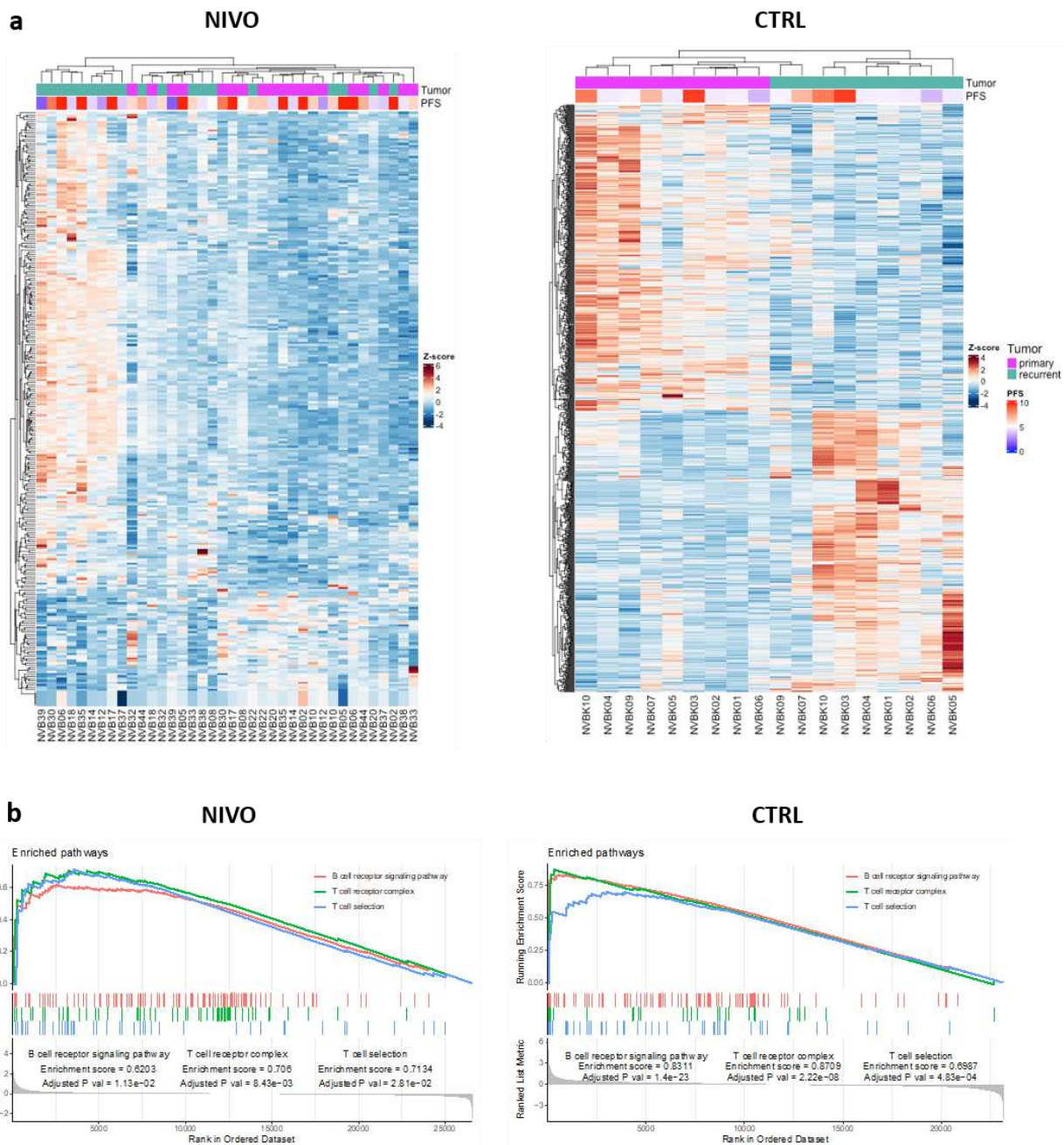
Inhibitory checkpoint molecules



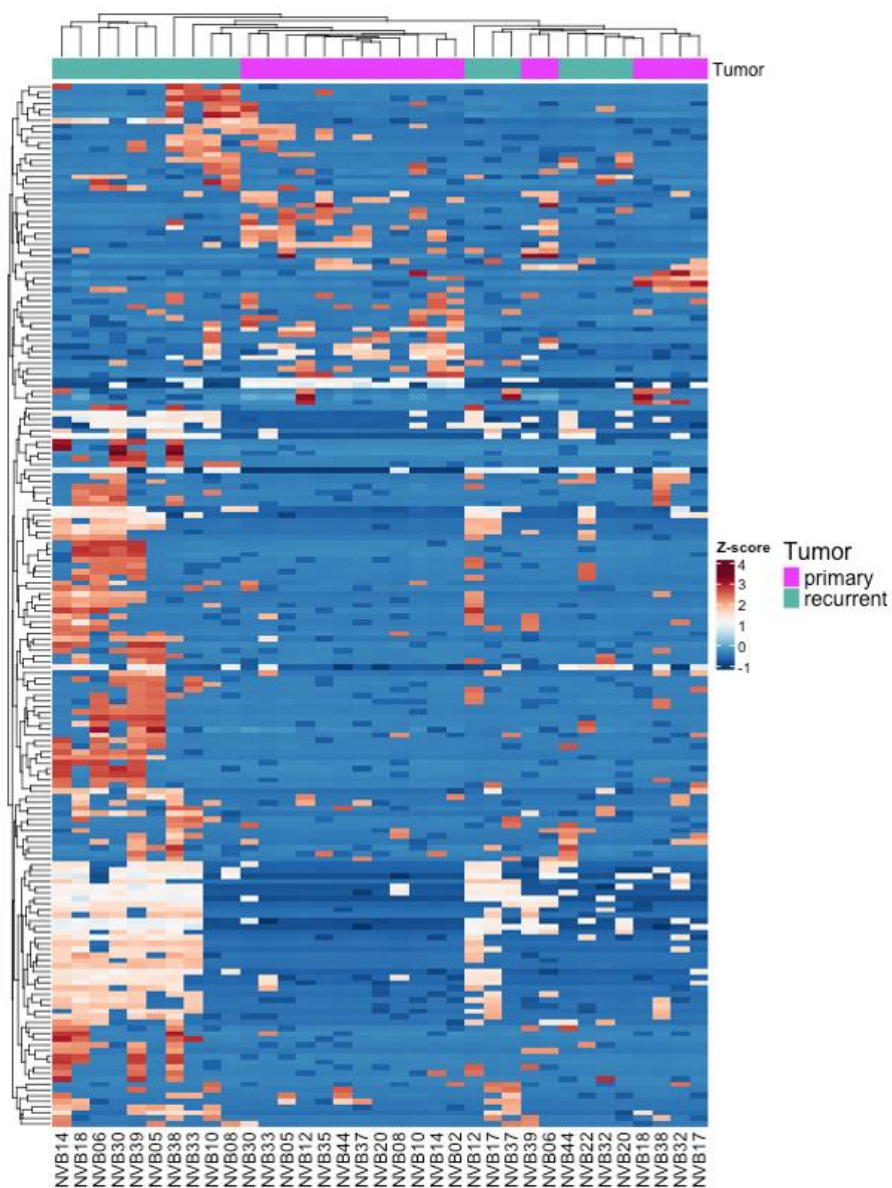
Supplementary Figure 3 CNS homing - and activation markers and inhibitory checkpoint molecules on PBMC derived T-cells. Frequency of CD8+ and CD4+T-cells expressing various markers and molecules in blood samples from T1 (Day 0), T2 (3 weeks), T3 (8 weeks) and T4 (16 weeks).



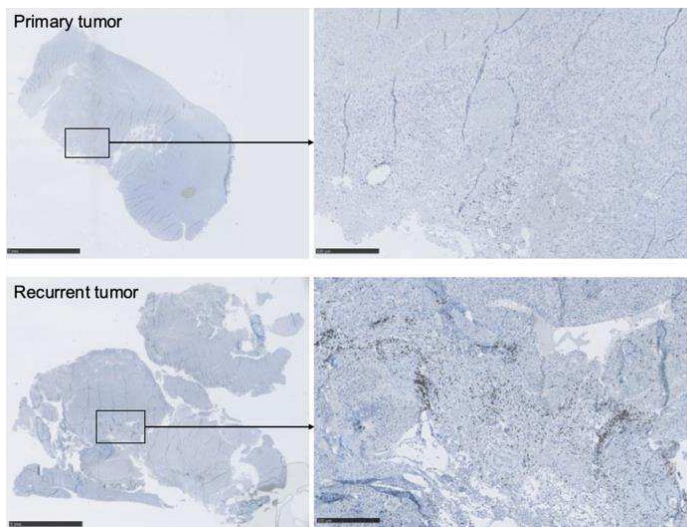
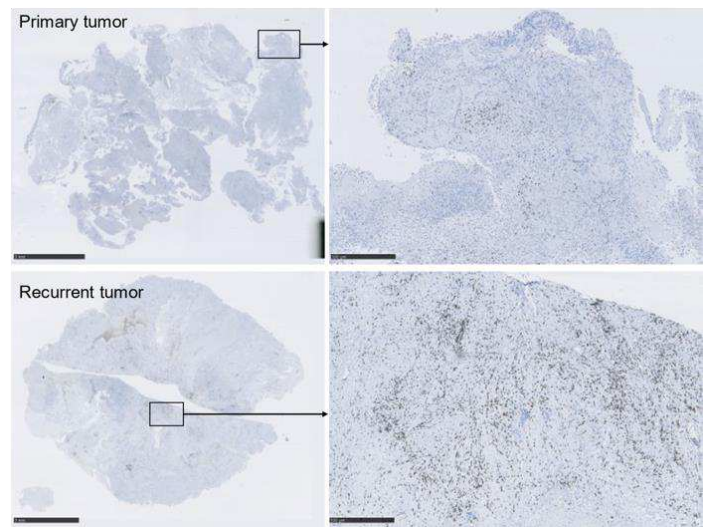
Supplementary Figure 4 Progression free survival and overall survival related to frequency of CD8+ T-cells expressing CD28. Kaplan-Meier curve of progression free survival (PFS) and overall survival (OS) in the recurrent setting for patients with high and low frequency of intratumoral CD8+ T-cells expressing CD28 within both Nivolumab-treated (NIVO) and control (CTRL) patients.



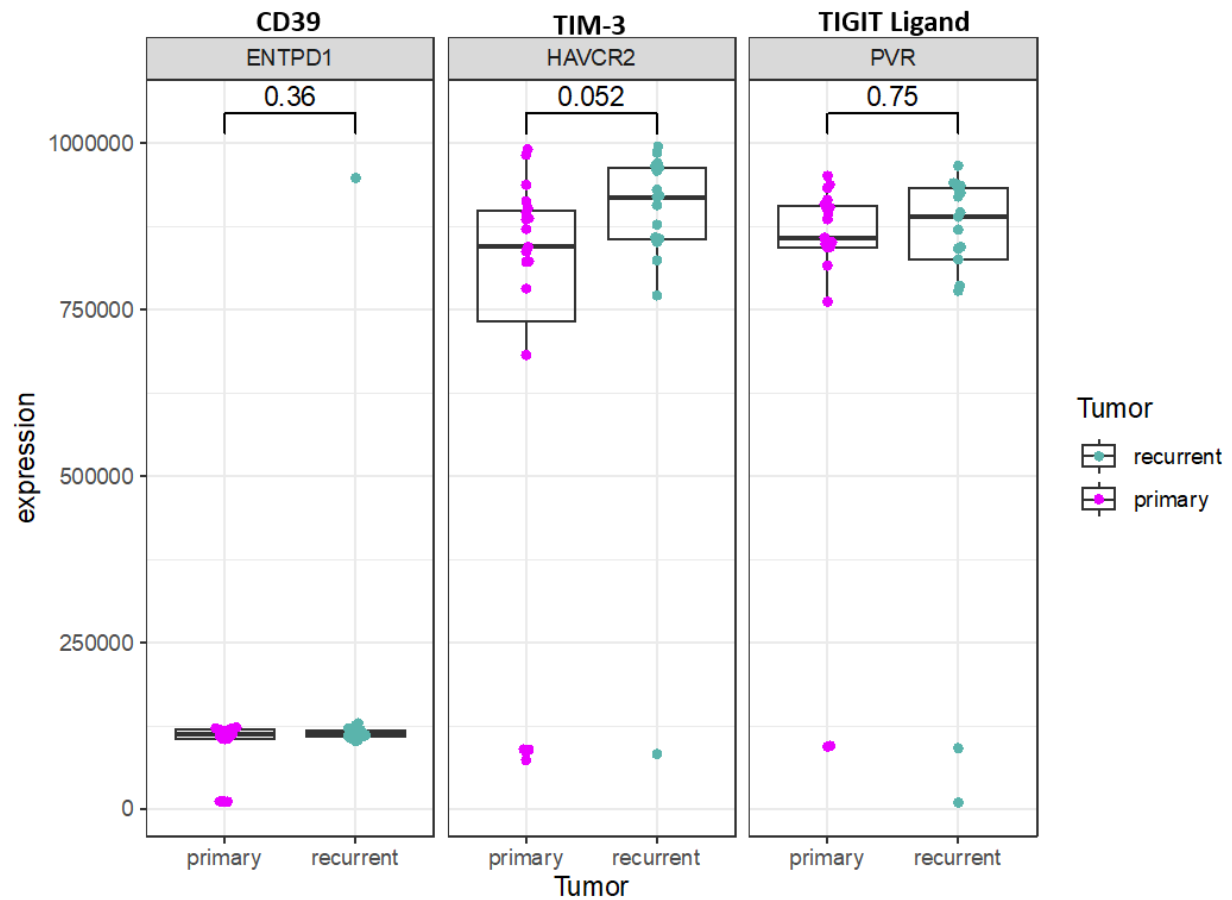
Supplementary Figure 5 Transcriptomic comparison of primary and recurrent tumor samples. a) Significantly differential expressed (DE) genes with adjusted p-value < 0.05 and log2 fold change > 1 or < -1 were illustrated with a heatmap with unsupervised clustering. Heatmaps are shown for both patients treated with Nivolumab (NIVO) containing 292 DE genes and control patients (CTRL) with 957 DE genes. **b)** A gene set enrichment analysis showed that genes related to the B cell receptor signaling pathway, T-cell receptor complex and T-cell selection were differential over-expressed in recurrent tumor samples compared to samples from primary tumor, for both the NIVO group and the CTRL group.



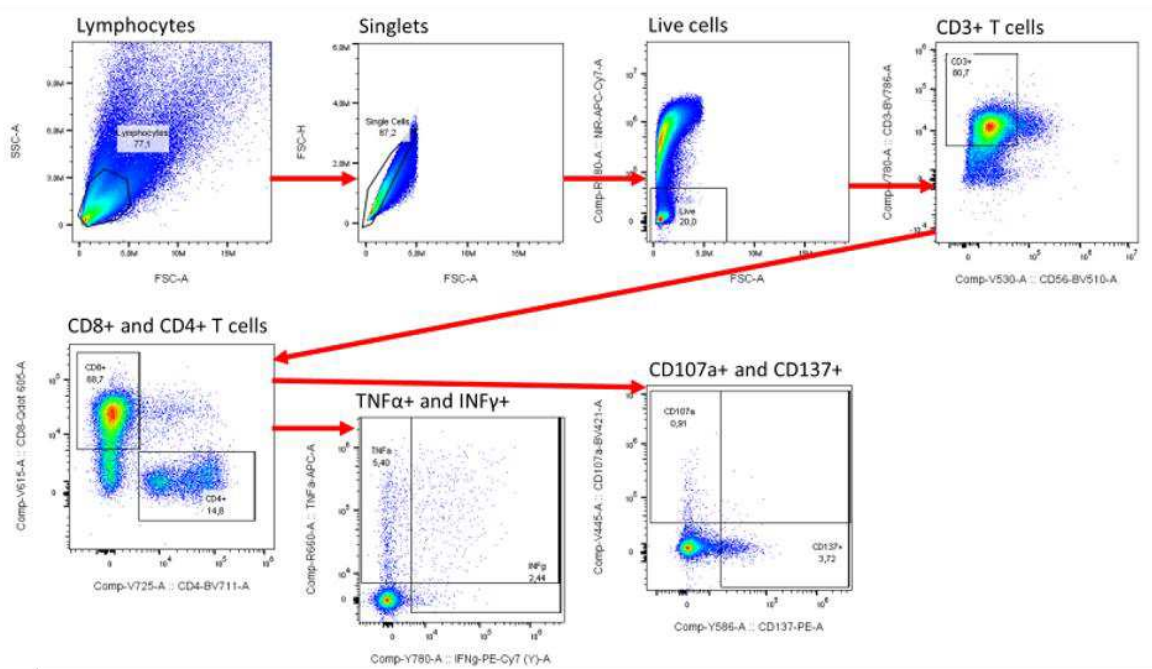
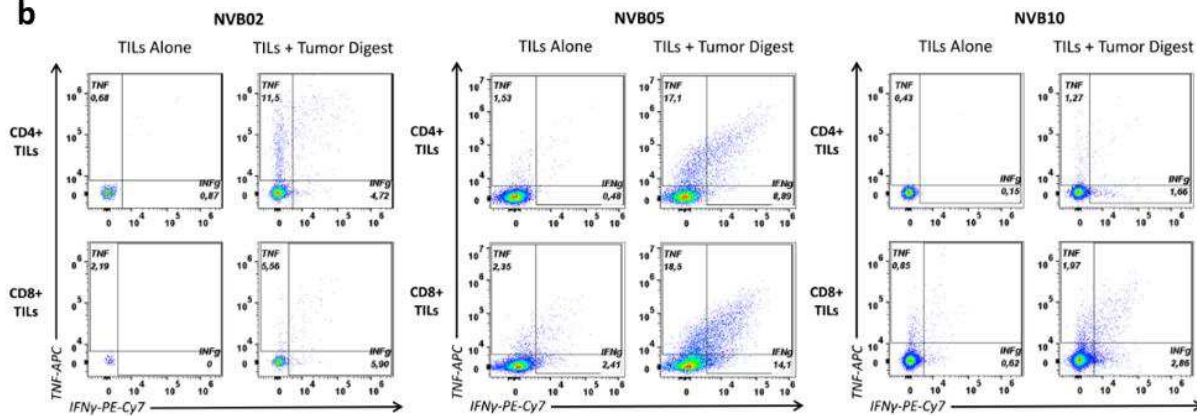
Supplementary Figure 6 Proteomics comparison of primary and recurrent tumor samples. 185 significantly differential expressed proteins with adjusted p-value < 0.05 were illustrated with a heatmap with unsupervised clustering. Heatmap is shown for patients treated with Nivolumab in the recurrent setting (NIVO).

NVB20**NVB30**

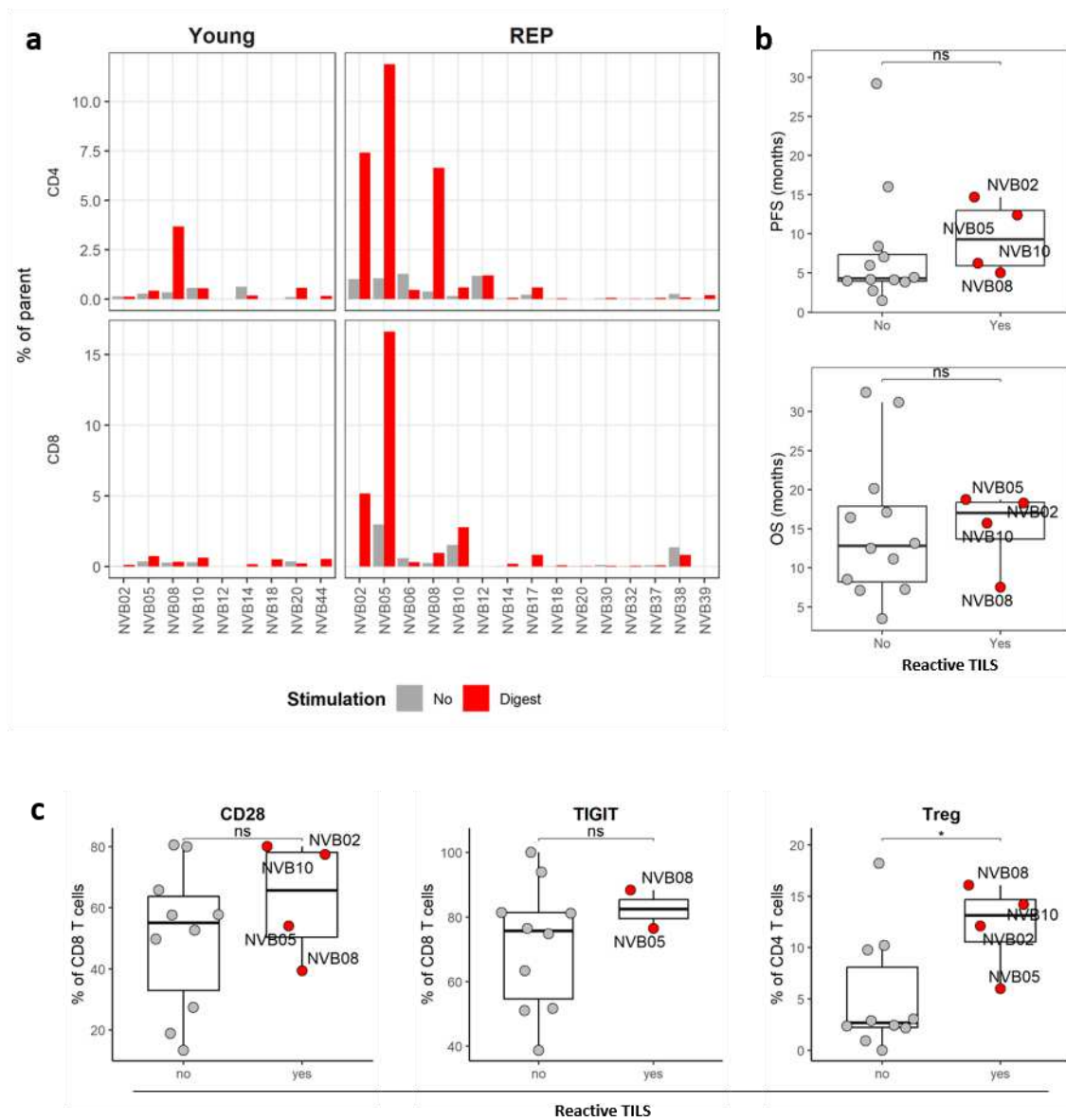
Supplementary Figure 7 Paired glioblastoma samples from primary and recurrent tumor both stained for CD3+ cells (T-cells). The recurrent tumor has been exposed to one dose of Nivolumab seven days prior to salvage resection. In the recurrent tumor we found a higher level of T-cell infiltration than in the corresponding primary tumor. Scale bars = 5 mm (left), and 500 μ m (right)



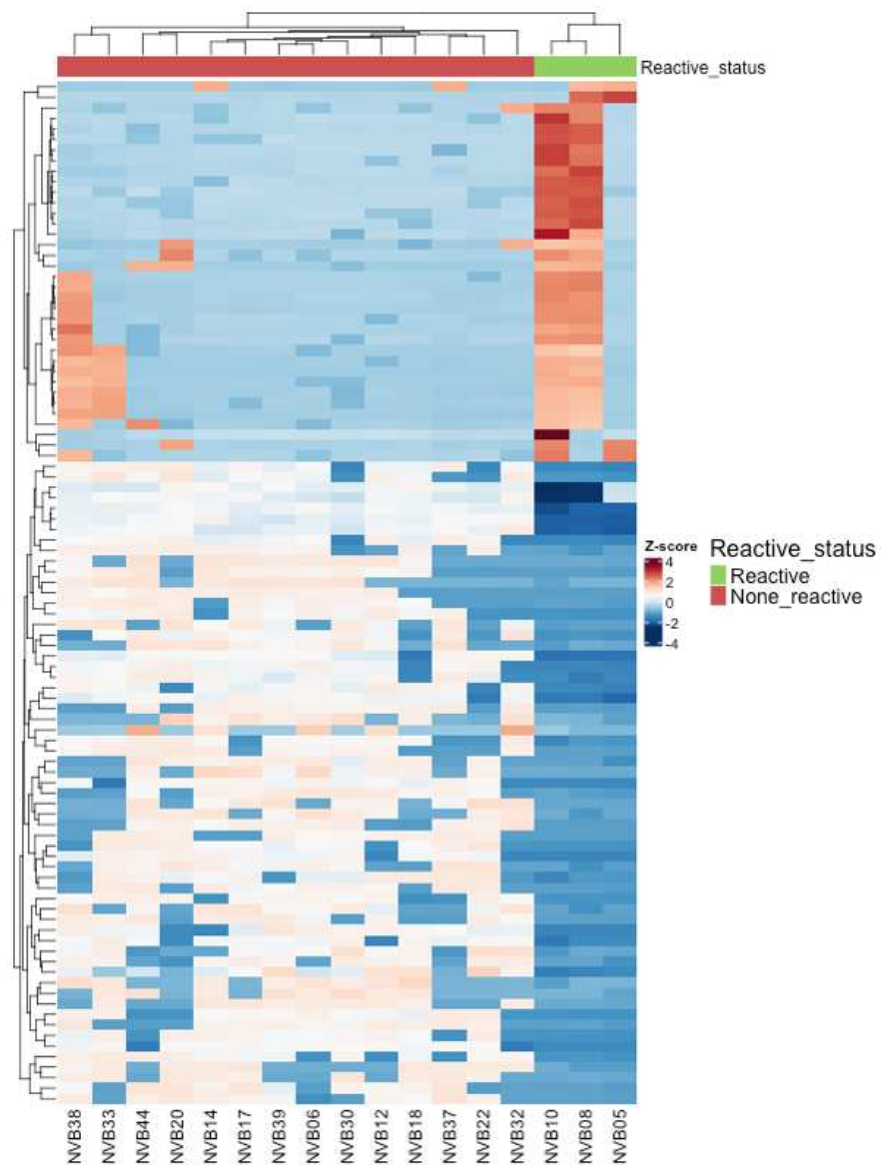
Supplementary Figure 8 Selected protein expression in primary and recurrent tumor. Proteomic data was analyzed for expression of CD39, TIM-3 and PVR (CD155, the ligand of TIGIT). Data from primary and recurrent tumors were compared with in the patient group who received Nivolumab in the recurrent setting (NIVO group). A tendency of upregulation of TIM-3 expression (p-value = 0.052, unpaired Wilcox test) was found in recurrent tumor after Nivolumab treatment. The expression of CD39 and PVR was detected in same levels in primary and recurrent tumors.

a**b**

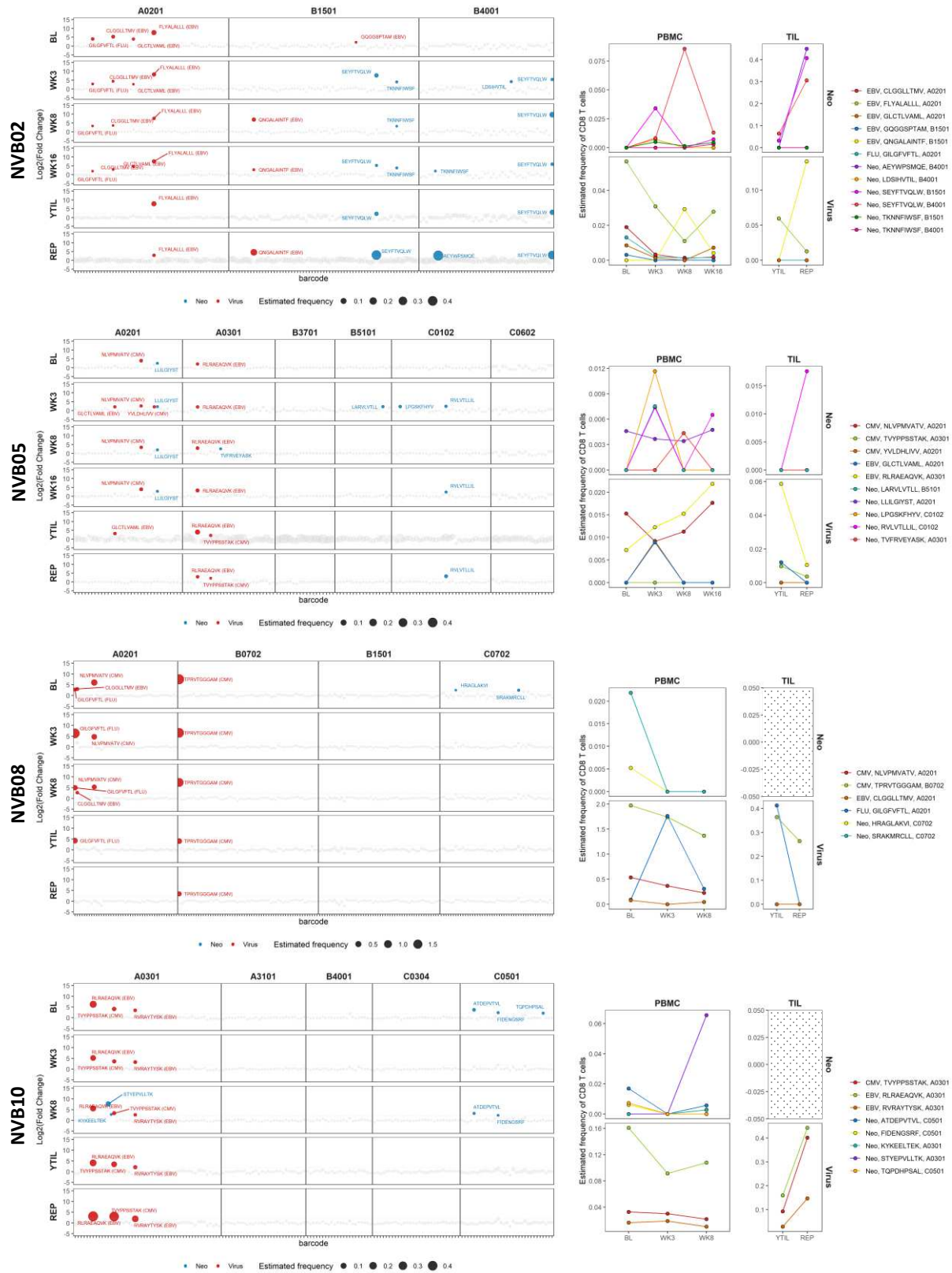
Supplementary Figure 9 Gating strategy for T-cell reactivity assay. TILs were co-cultured with autologous tumor digest for 8 hours and hereafter intracellularly stained for TNF-α, IFN-γ, CD137 and surface staining for CD107a. **a)** Gating strategy of TILs in the reactivity assay. **b)** Flow cytometry dotplot for patient with tumor-reactive TILs, showing TNF-α and IFN-γ expression in CD4+ and CD8+ T-cells after co-culture with autologous tumor digest or TILs alone.



Supplementary Figure 10 Tumor-reactive TILs. **a)** Frequency of tumor reactive TILs raw data; reactivity in Young TILs (YTILs) and REP TILs including background reactivity (TILs alone, grey) and co-cultures with tumor digest (red) for all tested patients. **b)** Progression free survival (PFS) and overall survival (OS) in a recurrent setting stratified in reactive (Yes) and non-reactive (No) patients within the Nivolumab-treated (NIVO) patient group. **c)** Frequency of intratumoral CD8+ T-cells expressing CD28 and TIGIT, and frequency of Treg cell among CD4+ T-cells stratified in reactive and non-reactive patient within the NIVO patient group. Means were compared between patients with reactive and non-reactive TILs using unpaired t-test. * = $p < 0.05$, ** = $p < 0.01$, *** = $p < 0.001$, **** = $p < 0.0001$.

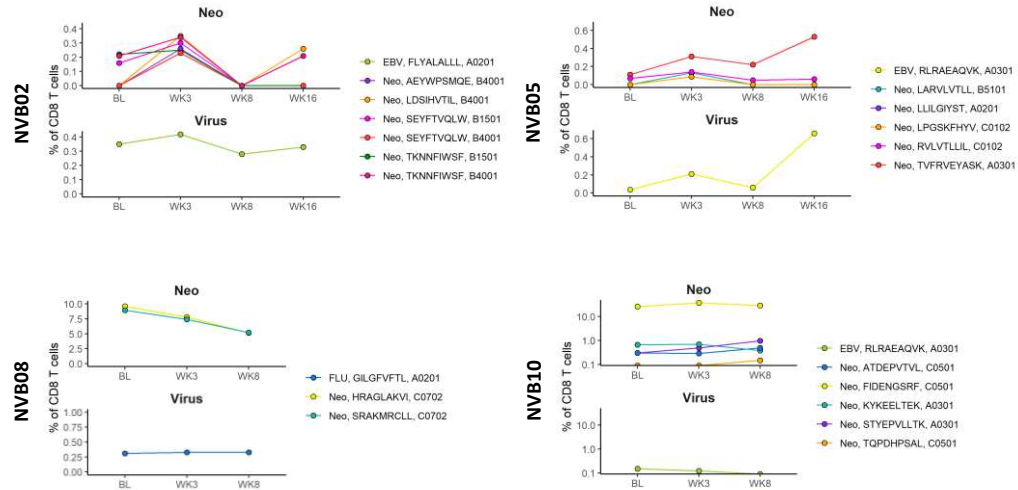


Supplementary Figure 11 Proteomics comparison of samples from patients with tumor reactive and non-reactive TILs in the Nivolumab treated patient group. 58 differential over-expressed and 34 differential under-expressed proteins were found in patients with reactive T-cells by differential expression analysis with adjusted p-value < 0.05. These differential expressed proteins were illustrated by heatmap showing that patients with reactive and non-reactive T-cells were defining the two first unsupervised clusters. 22 proteins overlapped with genes from the transcriptomics results.

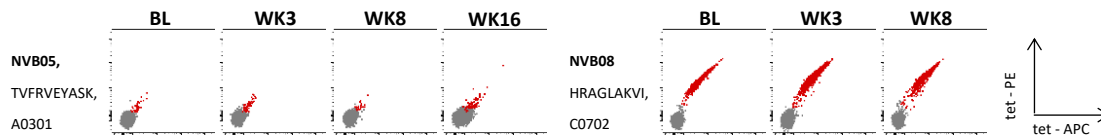


Supplementary Figure 12 Detection of NARTs in YTILs, REP TILs and ex vivo PBMCs. Screening output for all patients with reactive TILs. Significantly enriched ($p < 0.001$, Log_2 fold change > 2) barcoded pMHC multimers are colored and labelled with the immunogenic peptide sequence. Virus antigens are marked in red and neoantigens are marked in blue. The dot size represents an estimated frequency of CD8+ T-cells for each NART. Grey dots are all pMHC multimers that were not significantly enriched after sample staining. Specificities are shown for each blood sample time point; baseline (BL), week (WK) 3, WK8, WK16, and for YTIL (young TILs) and REP TILs. The screened pMHC are additionally divided based on HLA type (left). The estimate frequency is shown for each specificity in PBMCs and TILs (right).

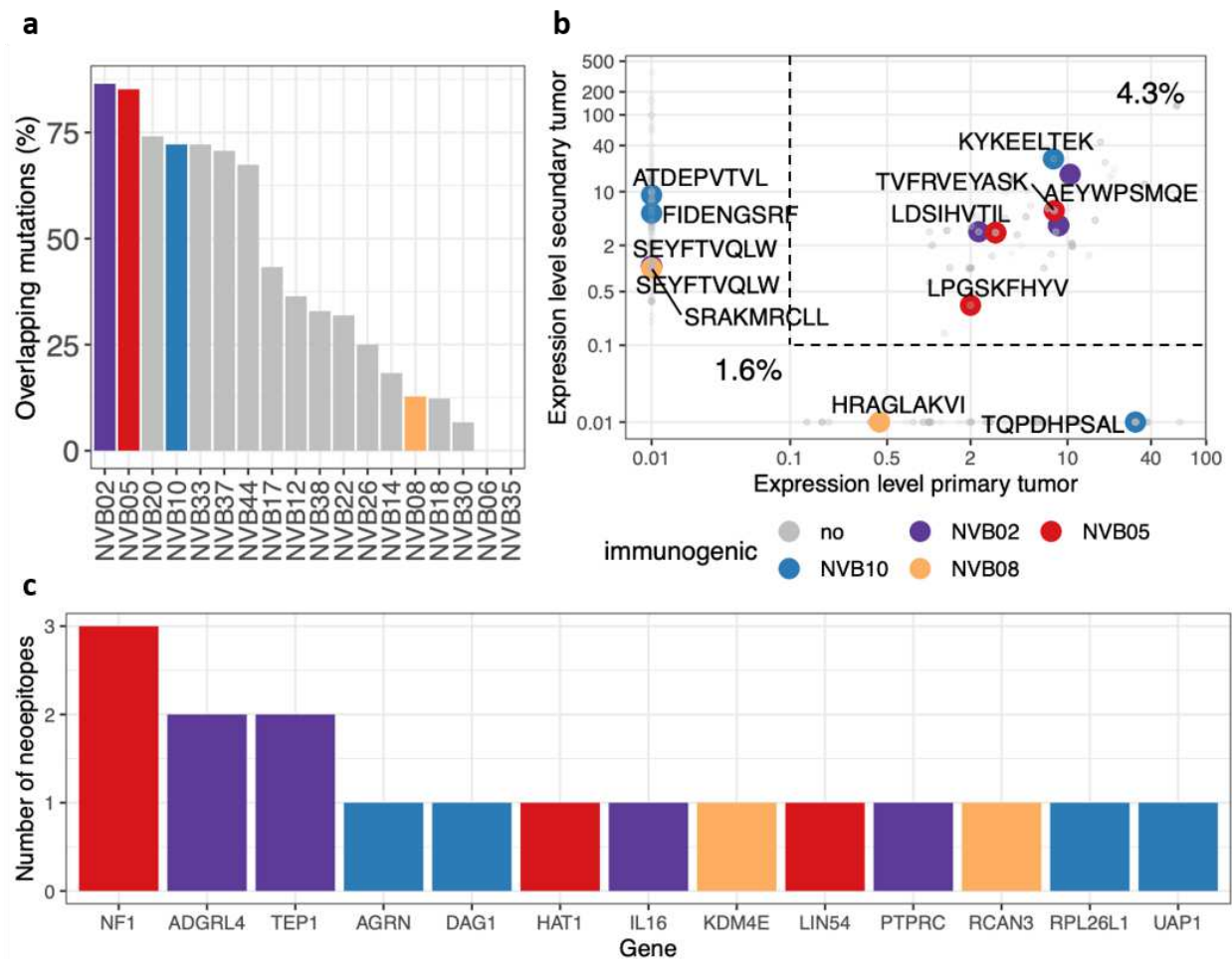
a



b



Supplementary Figure 13 Verification of detected NARTs. PBMCs were expanded with a pool of the detected immunogenic peptides over 14 days. Expanded PBMCs were hereafter stained with pMHC tetramers specific for the immunogenic peptides. **a)** Frequencies of expanded NART within CD8+ T-cells from expanded PBMCs deriving from the blood sample time points, baseline (BL), week (WK) 3, WK8 and WK16. **b)** Representative plots for expanded NARTs from patient NVB05 and NVB08.



Supplementary Figure 14 Immunogenic vs. non-immunogenic neoepitopes. **a)** Frequency of mutations overlapping between primary and recurrent tumor. **b)** Expression level of the mutation found in primary vs. secondary tumor. 4.3 % of the peptides, which are found in both primary and secondary tumors, are found immunogenic, whereas only 1.6 % of peptide found in only one of the tumor samples are found immunogenic ($p=0.06$, with a proportion z-test). Grey dots represents screened non-immunogenic peptides, and the colored dots represents immunogenic peptides. **c)** The number of immunogenic neoepitopes within the gene the mutation appeared.

Supplementary Tables

Supplementary Table 1 Tissue overview

Pseudonym	Tumor digest (single cell suspension)	Young TILs ¹	REP TILs ¹	Tumor cell line
NVB02	x	x	x	Not available
NVB05	x	x	x	X
NVB06	x	x	x	Failed
NVB08	x	x	x	Not available
NVB10	x	x	x	Not available
NVB12	x	x	x	Not available
NVB14	x	x	x	Failed
NVB17	x	Not available	x	Not available
NVB18	x	x	x	Not available
NVB20	x	x	X	Not available
NVB22	x	x	Failed	Not available
NVB26	x	x	Not possible ²	Failed
NVB30	x	Not possible ²	x	Not available
NVB32	x	X	x	Not available
NVB33	Not available	Not possible ²	Not possible ²	Not available
NVB35	x	x	Failed	Not available
NVB37	x	Not possible ²	x	Not available
NVB38	x	Failed	x	Not available
NVB39	x	x	x	Not available
NVB44	x	x	x	Not available
K_01	X	X	X	Not available
K_02	X	X	X	Not available
K_03	X	X	X	Not available
K_04	X	X	X	Not available
K_05	X	X	X	Not available
K_06	X	X	X	Not available
K_07	X	X	X	Not available
K_08	X	X	X	Not available
K_09	X	Failed ²	X	Not available
K_10	x	Failed ²	X	Not available

¹Tumor Infiltrating Lymphocytes, ²Due to limited tumor sample size.

Supplementary Table 2 Presentation of patients included in CA209-9UP.

	Surgical group	Non-surgical group
	N =20 (100.0%)	N =20 (100.0%)
Median age	57.5 years	50.5 years
Gender		
Female	8 (40.0)	8 (40.0)
Male	12 (60.0)	12 (60.0)
Performance status WHO		
0	18 (90.0)	18 (90.0)
1	2 (10.0)	2 (10.0)
MGMT unmethylated*	9 (45.0)	11 (55.0)
IDH mutant**	3 (15.0)	5 (25.0)
Multifocal disease at recurrence		
Yes	1 (5.0)	3 (15.0)
No	19 (95.0)	17 (85.0)
Extent of surgical resection at primary diagnosis		
Total resection	15 (75.0)	10 (50.0)
Partial resection/biopsy	3 (15.0)	7 (35.0)
Unknown	2 (10.0)	3 (15.0)
Steroid use at inclusion in the trial		
No use	16 (80.0)	15 (75.0)
≥10 - ≤ 20 mg daily	4 (20.0)	5 (25.0)
Steroid use at third cycle treatment		
No use	12 (60.0)	11 (55.0)
≥10 - ≤ 20 mg daily	5 (25.0)	4 (20.0)
Never received third cycle	3 (15.0)	5 (25.0)

N = number. *= Cut-off value for methylated/un-methylated was 10% methylation. **= Both IDH mutant 1 and 2 included.

Supplementary Table 3 Toxicity among patients in CA209-9UP.

	Surgical group			Non-surgical group	
	N = 20			N = 20	
	Grade 3 (%)	Grade 4 (%)		Grade 3 (%)	Grade 4 (%)
Event					
Hypertension	1	0		0	0
Arthralgia	0	0		0	0
Headache	0	0		0	0
Fatigue	0	0		0	0
Infection	4	0		0	0
Proteinuria	0	0		0	0
Diarrhea	1	0		0	0
Seizures	2	0		0	0
Anorexia	0	0		0	0
Hyperglycemia	0	0		0	0
Neutropenia	1	0		0	0
Fever	1	0		0	0
Vasculitis	1	0		0	0
SAH*	0	0		1	0
PRES**	1	0		0	0

*Subarachnoid hemorrhage, **Posterior reversible encephalopathy syndrome, classified as a SUSAR (Suspected Unexpected Serious Adverse Reaction). CTCAE version 4.03 was used.

Supplementary Table 4 Multivariate analysis of CA209-9UP patients (N=40).

Parameter		Parameter Estimate	Standard Error	Chi-Square	Pr > ChiSq	Hazard Ratio	95% Hazard Ratio Confidence Limits	
MGMT status	Unmethylated	0.31878	0.39247	0.6597	0.4167	1.375	0.637	2.968
Patient group	Surgical	-0.95444	0.41195	5.368	0.0205	0.385	0.172	0.863
Gender	Female	0.61014	0.4152	2.1594	0.1417	1.841	0.816	4.153
Steroid	Yes	0.90557	0.4404	4.2281	0.0398	2.473	1.043	5.863
Age at diagnosis	per 10 yrs	-0.02721	0.01924	2.0004	0.1573	0.973	0.937	1.011

Supplementary Table 5 Inclusion and exclusion criteria of the protocol

Inclusion criteria	<ol style="list-style-type: none"> 1. Pathologically confirmed GBM (including all histologic variants). 2. Age \geq 18 years. 3. Evidence of radiological (MRI-scan) measurable recurrent progressive GBM evaluated by the Response Assessment in Neuro-Oncology [RANO] criteria. 4. In arm B measurable disease according to the RANO guidelines, within 14 days of starting treatment. Measurable disease after surgery on arm A is not required with radiographic evidence of recurrent disease after treatment with temozolomide and radiotherapy. 5. An interval of at least 4 weeks between prior radiotherapy or chemotherapy and enrolment on this protocol. 6. Eastern Cooperative Oncology Group (ECOG) Performance Status (PS) 0-2. 7. Life expectancy, in the opinion of the investigator \geq 3 months. 8. Written informed consent obtained prior to any screening procedures. Patients must be willing and able to comply with the protocol and aware of the investigational nature of this study. 9. Patients must have adequate bone marrow function and organ function within 2 weeks of study treatment as defined by the following laboratory criteria. <ol style="list-style-type: none"> a. Hematopoietic function: total white blood cell count (WBC) \geq 3000/mm³, absolute neutrophil count (ANC) \geq 1500/mm³, platelet count \geq 125,000/mm³; hemoglobin \geq 9g/dL b. Hepatic function: bilirubin < 1.5 times the upper limit of normal (ULN) (excluding Gilberts Syndrome, for which bilirubin must be \leq 4 times ULN), ALAT < 2.5 times ULN. c. Renal function: serum creatinine < 1.5 ULN or estimated creatinine clearance of \geq 50 mL/min, calculated using the formula of Cockcroft and Gault. d. APTT and INR < normal limit 10. All female patients and partners of childbearing potential must agree to use adequate birth control during study treatment and for 5 months after the last dose of study drug and have a negative serum pregnancy test at screening. Acceptable methods of contraception are oral, implantable, or injectable contraceptives, contraceptive patch, intrauterine device, or a sexual partner who is surgically sterilized or post-menopausal. 11. Fertile males must be willing to employ adequate means of contraception during study treatment and for 7 months after the last dose of study drug. 12. Archived paraffin-embedded tissue (approximately 10 unstained slides or a tumor block) must be available for confirmation of tumor diagnosis and correlative studies. 13. Patients in the surgical arm (Arm A) must be predicted pre-operatively to have sufficiently sized recurrent tumor to allow for 500 mg of enhancing tumor and 300 mg of non-enhancing tumor to be resected. 14. Patients must be on a stable or decreasing dose of corticosteroids (or none) for at least 5 days prior to MRI and maximum of a dose of 20 mg prednisolone per day at enrollment of the study.
--------------------	---

Exclusion criteria	<ol style="list-style-type: none"> 1. Patients must not have significant medical illness that in the investigator's opinion cannot be adequately controlled with appropriate therapy or would compromise the patient's ability to tolerate this therapy. 2. Co-medication that may interfere with study results, e.g. immuno-suppressive agents other than corticosteroids (equivalent to max dose of 20 mg prednisolone per day) and stable for at least 5 days prior to day 1; 3. Any condition (medical, social, psychological), which would prevent adequate information and follow-up. 4. Any other active malignancy or previous malignancies within the last 5 years, except, adequately treated basal or squamous cell carcinoma of the skin, or carcinoma in situ. 5. Uncontrolled hypertension (systolic blood pressure (BP) > 150 mmHg and/or diastolic BP > 100 mmHg), unstable angina, congestive heart failure (CHF) of any New York Heart Association (NYHA) classification, serious cardiac arrhythmia requiring treatment (exceptions: atrial fibrillation, paroxysmal supraventricular tachycardia), history of myocardial infarction within 6 months of enrollment. 6. Clinically significant peripheral vascular disease 7. Evidence of bleeding diathesis, coagulopathy or taking ASA, NSAIDs or clopidogrel. 8. Patients with coagulation problems and medically significant bleeding in the month prior to start of treatment (e.g., peptic ulcer, epistaxis, spontaneous bleeding). 9. Major surgical procedure, open biopsy, or significant traumatic injury within 28 days prior to day 0, anticipation of need for major surgical procedure during the course of the study. 10. Minor surgical procedures, fine needle aspirations or core biopsies within 7 days prior to day 0. 11. History of abdominal fistula, gastrointestinal perforation, or intra-abdominal abscess within 6 months prior to day 0. 12. Known active hepatitis A, B or C infection; or known to be positive for HCV RNA or HBsAg (HBV surface antigen); hepatitis testing is not required. 13. Known HIV infection; HIV testing is not required. 14. Active infection requiring parenteral systemic antibiotics. 15. Administration of a live, attenuated vaccine within 4 weeks before first dose of Nivolumab prior to surgery in Arm A or Cycle 1 Day 1 (Arm A and B) or anticipation that such a live attenuated vaccine will be required during the study. Influenza vaccination should be given during influenza season only (approximately October to March). Patients must not receive live, attenuated influenza vaccine (e.g., FluMist®) within 4 weeks before first dose of Nivolumab prior to surgery in Arm A or Cycle 1 Day 1 (Arm A and B) or at any time during the study. 16. Severe infections within 4 weeks prior to Cycle 1 Day 1, including but not limited to hospitalization for complications of infection, bacteremia, or severe pneumonia. 17. Received oral or intravenous (IV) antibiotics within 2 weeks prior to Cycle 1 Day 1. Patients receiving prophylactic antibiotics (e.g., for prevention of a
--------------------	--

urinary tract infection or chronic obstructive pulmonary disease) are eligible.

18. Any other diseases, metabolic dysfunction, physical examination finding, or clinical laboratory finding giving reasonable suspicion of a disease or condition that would contraindicate the use of an investigational drug;
19. Dementia or altered mental status that would prohibit informed consent.
20. History of organ allograft.
21. History or risk of autoimmune disease, including but not limited to systemic lupus erythematosus, rheumatoid arthritis, inflammatory bowel disease, vascular thrombosis associated with antiphospholipid syndrome, Wegner's granulomatosis, Sjogren's syndrome, Bell's palsy, Guillain-Barre syndrome, multiple sclerosis, vasculitis, or glomerulonephritis.
22. History of idiopathic pulmonary fibrosis, pneumonitis (including drug induced), organizing pneumonia (i.e., bronchiolitis obliterans, cryptogenic organizing pneumonia, etc.), or evidence of active pneumonitis on screening chest CT scan. History of radiation pneumonitis in the radiation field (fibrosis) is permitted.
23. Pregnant or breast-feeding women.
24. Prior treatment with PD-1/PD-L1 inhibitors.
25. Known hypersensitivity to any of the components of Nivolumab or Bevacizumab.
26. Investigational therapy (defined as treatment for which there is no regulatory authority; within 28 days prior to Cycle 1 Day 1.
27. Any approved anti-cancer therapy, including chemotherapy or hormonal therapy, within 3 weeks prior to Cycle 1 Day 1, with the following exceptions:
 - a. Hormone-replacement therapy or oral contraceptives
28. Treatment with systemic immunosuppressive medications including, but not limited to cyclophosphamide, azathioprine, methotrexate, thalidomide, and anti-TNF agents within 2 weeks prior to Cycle 1, Day 1. The use of inhaled corticosteroids and mineralocorticoids (e.g., fludrocortisone) for patients with orthostatic hypotension or adrenocortical insufficiency is allowed.
29. Concurrent therapy with approved or investigational anticancer therapeutics.
30. Body weight significantly below ideal body weight in the opinion of the investigator.

Supplementary Table 6 Fluorochrome panel overview

Marker	Flouorochrome	Clone	Dilution	Company	Type
Panel A: Activated T cells					
CD3	FITC	SK7	1:10	BD Biosciences	Surface
CD4	BUV395	M-T477	1:320	BD Biosciences	Surface
CD8	BV480	RPA-T8	1:80	BD Biosciences	Surface
CD28	BUV737	CD28.2	1:80	BD Biosciences	Surface
CD39	BV786	TU66	1:40	BD Biosciences	Surface
CD45RA	BV421	HI100	1:160	BD Biosciences	Surface
CD69	PE-Cy7	L78	1:40	BD Biosciences	Surface
CD103	PerCP eFlour710	Ber-ACT8	1:20	Invitrogen	Surface
CD137	PE-Cy5	4B4-1	1:40	BD Biosciences	Surface
CD183 (CXCR3)	BV711	G025H7	1:40	Biolegend	Surface
CD197 (CCR7)	APC	G043H7	1:20	Biolegend	Surface
CD279 (PD1)	PE-CF594	EH12.1	1:80	BD Biosciences	Surface
IgG4	PE	HP6025	1:40	SouthernBiotech	Surface
CD195(CCR5)	BV650	3A9	1:40	BD Biosciences	Surface
Live	NiR		1:1000	Invitrogen	Surface
Panel B: Exhausted T cells and Tregs					
CD3	FITC	SK7	1:10	BD Biosciences	Surface
CD4	BUV395	M-T477	1:320	BD Biosciences	Surface
CD8	BV480	RPA-T8	1:80	BD Biosciences	Surface
CD25	BV711	BC96	1:40	Biolegend	Surface
CD45RA	BV421	HI100	1:160	BD Biosciences	Surface
		HIL-7R-			
CD127	APC-R700	M21	1:40	BD Biosciences	Surface
CD152 (CTLA-4)	PE-Cy5	BNI3	1:20	BD Biosciences	Surface
CD197 (CCR7)	APC	G043H7	1:20	Biolegend	Surface
CD223 (LAG-3)	BV650	11C3C65	1:160	Biolegend	Surface
CD279 (PD1)	PE-CF594	EH12.1	1:80	BD Biosciences	Surface
CD366 (TIM-3)	PE-Cy7	F38-2E2	1:80	Biolegend	Surface
FoxP3	PE	259D/C7	1:10	BD Biosciences	IC
Ki67	BV786	B56	1:40	BD Biosciences	IC
TIGIT	BV605	A15153G	1:20	Biolegend	Surface
Live	NiR		1:1000		Surface
Panel C: Multicytokines Intracellular Staining Panel					
CD3	FITC	SK7	1:10	BD Biosciences	Surface
CD4	BUV395	M-T477	1:320	BD Biosciences	Surface
CD8	BV480	RPA-T8	1:80	BD Biosciences	Surface
TNF- α	PE-Cy7	MAB11	1:20	Biolegend	IC
IFN- γ	APC	25723.11	1:20	BD Biosciences	IC
CD137 (4-1BB)	BUV737	4B4-1	01:40	BD Biosciences	IC
Live	NiR		1:1000		Surface
Panel D: Multicytokines Intracellular Staining Panel					
CD137	PE	4B4-1		BD Biosciences	IC
IFN γ	PE-Cy7	B27		BD Biosciences	IC
TNF	APC	MAB11		BD Biosciences	IC
Live	APC-Cy7	None		Thermo Fisher Scientific	Surface
CD107a	BV421	H4A3		BD Biosciences	Surface
CD56	BV510	NCAM16.2		BD Biosciences	Surface
CD8	Qdot 605	3B5		Thermo Fisher Scientific	Surface
CD4	BV711	SK3		BD Biosciences	Surface
CD3	BV786	SK7		BD Biosciences	Surface